

Holstein model in infinite dimensions at half-filling

Patrizia Benedetti and Roland Zeyher

Max-Planck-Institut für Festkörperforschung,

Heisenbergstr.1, 70569 Stuttgart, Germany

(August 8, 2018)

Abstract

The normal state of the Holstein model is studied at half-filling in infinite dimensions and in the adiabatic regime. The dynamical mean-field equations are solved using perturbation expansions around the extremal paths of the effective action for the atoms. We find that the Migdal-Eliashberg expansion breaks down in the metallic state if the electron-phonon coupling λ exceeds a value of about 1.3 in spite of the fact that the formal expansion parameter $\lambda\omega_0/E_F$ (ω_0 is the phonon frequency, E_F the Fermi energy) is much smaller than 1. The breakdown is due to the appearance of more than one extremal path of the action. We present numerical results which illustrate in detail the evolution of the local Green's function, the self-energy and the effective atomic potential as a function of λ .

I. INTRODUCTION

Studies on the microscopic mechanism of high- T_c superconductivity and of the colossal magnetoresistance have shown the need for a more detailed investigation of simple models for the electron-phonon coupling. One generic model is the Holstein model¹ which consists of conduction electrons interacting locally with optical phonons. The case of just one electron has received a lot of attention in the past. In particular, the formation of small and large polarons and their motions have been studied considering both the adiabatic and the anti-adiabatic cases^{1–6}. However, the application of the obtained results to high- T_c superconductors⁷ or to the manganites⁸ is problematic. In these systems the Fermi energy E_F is substantially larger than typical phonon energies ω_0 . One thus deals in these systems with a large Fermi surface where the Migdal-Eliashberg⁹ self-consistent perturbation theory, governed by the small parameter $\lambda\omega_0/E_F$ (λ is the electron-phonon coupling constant), should be more appropriate than the use of canonical transformations typical for the one-electron problem.

From the studies on the single polaron problem it is known that polaron formation, i.e., the sudden and large mass enhancement of the electron, takes place around $\lambda \sim 1$. Associated with this is a breakdown of simple perturbation theory due to the appearance of a bound state in the electron-phonon system. Whether something similar happens in the case of many electrons and a large Fermi surface is still a matter of controversy. On the one hand, it has been argued that, due to the Migdal theorem, self-consistent theory works even if λ is not small. It is claimed that the only condition for the validity of the self-consistent perturbation theory is that $\lambda\omega_0/E_F \ll 1$ holds⁹. As a result many treatments in the past, for instance, for high- T_c superconductors, used values for λ which are much larger than 1¹⁰. On the other hand, it has been claimed that Migdal-Eliashberg perturbation theory breaks down if λ exceeds a critical value somewhere between 1 and 2, irrespective of the electronic density and the size of the Fermi surface¹¹. The arguments for this, however, were based on the Lang-Firsov transformation¹² which is more appropriate in the anti-adiabatic than

in the adiabatic limit and they seem to be supported by numerical calculations¹³. One aim of our contribution is to study the possible breakdown of Migdal-Eliashberg perturbation theory and polaron formation in the adiabatic regime where the hopping and the Fermi energy are much larger than the phonon energies. Another aim is the calculation of phonon renormalization effects caused by an arbitrarily strong electron-phonon coupling.

A suitable method to study the above problem is the dynamical mean-field theory^{14,15}. This method becomes exact in the limit of infinite spatial dimensions. It allows to map the lattice problem onto Anderson's single impurity problem embedded in an effective bath created by all the other sites and interacting with the electrons on the impurity in a dynamical, time-dependent way. In spite of the substantial simplifications introduced by infinite dimensions the resulting equations are in general still too complicated to admit exact analytic solutions. For the Holstein model some results from Monte Carlo simulations are available^{16–20}. Various approximate treatments have also been performed such as iterated perturbation theory¹⁹, self-consistent perturbation theory¹⁸ and the semiclassical approximation^{21,22}.

In the following we will formulate the dynamical mean-field equations in terms of path integrals. The phonon coordinate will not be treated as a classical variable without dynamics as in the semiclassical approach. Instead, we expand the path integrals around the paths which extremize the action. For small λ there is only one extremal and trivial path and Migdal-Eliashberg expansion is valid. Beyond a critical value for λ more than one extremal paths exist signalizing the breakdown of Migdal-Eliashberg theory though the system is still in the metallic state. Our treatment can be applied in the adiabatic regime to all coupling strengths λ and contains correctly the weak- and the strong-coupling cases. The paper is organized as follows: In section II the model and the dynamical mean-field equations are formulated. In section III the electrons are approximately integrated out in the path integral using a gradient expansion in time. The resulting effective action for the atoms is discussed. Approximate expressions for the electron Green's function are obtained in section IV. Section V contains numerical results for a Bethe lattice both for the atomic and the electronic properties. This section illustrates in detail the evolution of basic quantities

of the dynamical mean field theory such as the local Green's function, the electronic self-energy, the effective “unperturbed” Green's function and the effective atomic potential as a function of λ . Finally, section VI contains the conclusions.

II. MODELS AND DYNAMICAL MEAN-FIELD EQUATIONS

The Hamiltonian for the Holstein model can be written as¹

$$H = - \sum_{ij\sigma} t_{ij} (c_{i\sigma}^+ c_{j\sigma} + h.c.) + \frac{1}{2} \sum_i ((\partial_t \phi_i)^2 + \omega_0^2 \phi_i^2) + g \sum_{i\sigma} n_{i\sigma} \phi_i. \quad (1)$$

It describes a system of electrons interacting locally with dispersionless phonons. i, j denote the sites of a lattice, ω_0 is the frequency of the phonons, t_{ij} is the hopping matrix element of the electrons, and g the coupling constant between electrons and phonons. ϕ_i is the displacement operator of the atom at site i which can be expressed in terms of bosonic creation and annihilation operators a_i^\dagger, a_i as

$$\phi_i = \frac{1}{\sqrt{2\omega_0}} (a_i + a_i^\dagger). \quad (2)$$

$c_{i,\sigma}^\dagger, c_{i,\sigma}$ are creation and annihilation operators for electrons at site i and spin direction σ and $n_{i\sigma} = c_{i\sigma}^\dagger c_{i\sigma}$ is the density operator of electrons. The partition function of the model can be written as a path integral over anticommutating Grassmann numbers c^*, c (replacing the electronic operators), and phonon fields,

$$Z = \int D\phi Dc^* Dc e^{S[c^*, c, \phi]}, \quad (3)$$

where S is the action associated with the Hamiltonian (1).

In the limit of infinite spatial dimensions, $d \rightarrow \infty$, the dynamical mean-field approximation for H becomes exact. As a result the many-body problem Eq.(1) can be mapped onto an impurity model embedded in a dynamical bath¹⁴. Denoting the one-electron Green's function associated with the Hamiltonian of Eq.(1) by $G(\mathbf{k}, i\omega_n)$, the self-energy Σ is defined via Dyson's equation

$$G^{-1}(\mathbf{k}, i\omega_n) = G^{(0)-1}(\mathbf{k}, i\omega_n) - \Sigma(i\omega_n). \quad (4)$$

$G^{(0)}(\mathbf{k}, i\omega_n)$ is the free electron Green's function associated with the hopping term in Eq.(1). Using the Matsubara formalism ω_n are fermionic Matsubara frequencies $\omega_n = (2n + 1)\pi T$ where n is an integer and T the temperature. A very important simplification in infinite dimensions results from the fact that the self-energy Σ is independent of the momentum \mathbf{k} and depends only on the frequency¹⁵. The self-energy Σ also represents the self-energy of a site-independent impurity problem with the effective action S_{eff} given by

$$\begin{aligned} S_{eff} = & \int_0^\beta d\tau \int_0^\beta d\tau' \sum_\sigma c_\sigma^*(\tau) G_0^{-1}(\tau - \tau') c_\sigma(\tau') \\ & - \frac{1}{2} \int_0^\beta d\tau \phi(\tau) \left(-\frac{d^2}{d\tau^2} + \omega_0^2 \right) \phi(\tau) - g \int_0^\beta d\tau \sum_\sigma n_\sigma(\tau) \phi(\tau). \end{aligned} \quad (5)$$

G_0 describes a dynamical effective field acting on the impurity electrons due to the presence of all the other electrons in the crystal. It plays the role of a bare Green's function in S_{eff} and contains all the information on the influence of the surroundings on the impurity electrons. β in Eq.(5) stands for the inverse temperature $1/T$. Denoting the exact one-electron Green's function associated with S_{eff} by G_{loc} Dyson's equation of the impurity problem reads

$$G_{loc}^{-1}(i\omega_n) = G_0^{-1}(i\omega_n) - \Sigma(i\omega_n). \quad (6)$$

Finally, the so far unknown function G_0 is determined by the condition that G_{loc} coincides with the local Green's function calculated from the lattice Green's function $G(\mathbf{k}, i\omega_n)$, i.e.,

$$G_{loc}(i\omega_n) = \int d\epsilon \frac{N(\epsilon)}{i\omega_n - \epsilon + \mu_0 - \Sigma(i\omega_n)}. \quad (7)$$

μ_0 is the bare chemical potential and $N(\epsilon)$ is the bare density of electron states associated with the original hopping term in Eq.(1). In the following we will mainly consider the semicircular density of states of the Bethe lattice²³ given by

$$N(\epsilon) = \frac{\sqrt{(4t^2 - \epsilon^2)}}{2\pi t^2}. \quad (8)$$

This lattice has an infinite coordination number $z \rightarrow \infty$ and a rescaled nearest-neighbor hopping term $t_{ij} = t/\sqrt{z}$. In this particular case the relation between G_0 and G_{loc} becomes

$$G_0^{-1}(i\omega_n) = i\omega_n + \mu_0 - t^2 G_{loc}(i\omega_n). \quad (9)$$

Another popular density of states function is that of the Lorentz model

$$N(\epsilon) = \frac{t}{\pi(\epsilon^2 + t^2)}. \quad (10)$$

It describes a model with infinite range hopping terms and a function G_0 which simply is given by

$$G_0(i\omega_n) = i\omega_n + \mu_0 + it sgn \omega_n. \quad (11)$$

G_0 decouples in this case from all the other quantities. This model is therefore especially simple allowing often analytic expressions which capture essential features of models with more realistic density of states functions. On the other hand it misses the feedback from the other quantities and thus is unable to describe, for instance, the Mott-Hubbard transition from a metal to an insulator.

Eqs.(5)-(7) represent a closed set of equations. They have been derived under the assumption that no long-range order is present which will be assumed in the following. The above equations can be solved for large regions in parameter space numerically using Monte Carlo or diagonalization methods¹⁴. In the following we will use a more analytic method which gives directly some insight into the underlying physics.

III. EFFECTIVE ACTION FOR THE ATOMS

According to Eq.(5) S_{eff} is bilinear in the electronic variables. This means that the integration over electrons in the partition function Eq.(3) can be carried out yielding the following action S_{ph} for the phonon field alone:

$$S_{ph} = -\frac{1}{2} \int_0^\beta d\tau \phi(\tau) \left(-\frac{d^2}{d\tau^2} + \omega_0^2 \right) \phi(\tau) + Tr \log(G_0^{-1} - g\phi). \quad (12)$$

Here Tr means the trace over electronic variables, i.e., an integration over τ from 0 to β and a sum over the two spin components. The argument of the logarithm in Eq.(12) is a nondiagonal matrix consisting of the non-diagonal part G_0^{-1} and the diagonal part ϕ . Similarly, in ω_n -space the first contribution G_0^{-1} would be diagonal but the second one, ϕ would become non-diagonal.

Defining the expectation value of ϕ in the usual way by

$$\langle \phi \rangle = \int D\phi \phi e^{S_{ph}} / Z, \quad (13)$$

with

$$Z = \int D\phi e^{S_{ph}}, \quad (14)$$

there is no reason to expect that this static expectation value is zero even in the half-filled case. Indeed, writing down the equation of motion of Heisenberg operators using the original Hamiltonian Eq.(1) and considering the static limit we have

$$\langle \phi \rangle = -\frac{g}{\omega_0^2} \langle n \rangle. \quad (15)$$

$\langle n \rangle$ is the average number of electrons per site. It is therefore convenient to split ϕ into a static and a fluctuation part according to

$$\phi = \langle \phi \rangle + \tilde{\phi}, \quad (16)$$

where $\langle \phi \rangle$ is defined by the condition $\langle \tilde{\phi} \rangle = 0$. This shift can be interpreted as a Hartree term $\Sigma_H = g \langle \phi \rangle$ in the self-energy of G_0 . Since this term is frequency independent it just renormalizes the bare chemical potential as

$$\mu = \mu_0 - \Sigma_H. \quad (17)$$

From now on we will assume that this shift has been performed and that the chemical potential in G_0 is μ and no longer the bare one μ_0 .

The main problem left is the evaluation of the $Tr \log$ term in Eq.(12). For this we note that two independent parameters can be naturally defined in the Holstein model: one is the

electron-phonon coupling constant $\lambda = g^2/\omega_0^2 t$, and the other one is the adiabatic parameter $\gamma = \omega_0/t$. The adiabatic regime is defined by $\gamma \ll 1$, corresponding to the situation where the electrons move much faster than the phonons. For the calculation of the $Tr \log$ term we assume that $\gamma \ll 1$ holds. $\tilde{\phi}$ varies then slowly as function of τ compared with the variations in the electronic coordinates. An expansion in time gradients of $\tilde{\phi}$ represents thus an expansion in the Migdal parameter γ and we can confine ourselves to the lowest-order contributions.

Expanding the $Tr \log$ term in powers of g one obtains

$$Tr \log(G_0^{-1} - g\tilde{\phi}) = Tr \log G_0^{-1} - \sum_{n=1}^{\infty} \frac{1}{n} Tr(G_0 g\tilde{\phi})^n. \quad (18)$$

The first term on the right-hand side of Eq.(18) is independent of $\tilde{\phi}$ and thus will be dropped in the following. Writing the conservation of frequencies explicitly by means of a delta-function the general term of n -th order in g of the $Tr \log$ term becomes

$$X_n = -2 \frac{g^n}{n} T \sum_{\substack{\omega_1 \dots \omega_n \\ \nu}} \int_0^\beta d\tau e^{i(\omega_1 + \dots + \omega_n)\tau} \tilde{\phi}(\omega_1) G_0(\nu + \omega_1) \cdot \\ \tilde{\phi}(\omega_2) G_0(\nu + \omega_1 + \omega_2) \dots \tilde{\phi}(\omega_n) G_0(\nu + \omega_1 + \dots + \omega_n). \quad (19)$$

The prefactor 2 in Eq.(19) is due to the sum over the two spin directions. Due to the delta-function there are no restrictions in the sums over $\omega_1 \dots \omega_n$ in Eq.(19). For $\gamma \ll 1$ the motion of the atoms is slow compared to that of the electrons. In leading order in γ the electrons interact thus elastically with the phonons, i.e., they see the momentary value of the phonon field as a static field. This means that the phonon frequencies $\omega_1 \dots \omega_n$ can be neglected in the electron propagators G_0 . The sums over $\omega_1 \dots \omega_n$ can then trivially be carried out in Eq.(19). Summing also over n and adding the shifted harmonic potential the total potential $V(\tilde{\phi}(\tau))$ in S_{ph} becomes in this local approximation

$$V(\tilde{\phi}(\tau)) = \frac{\omega_0^2}{2} (\tilde{\phi}(\tau) + \langle \phi \rangle)^2 - 2T \sum_{\nu} e^{i\nu 0^+} \log(1 - g\tilde{\phi}(\tau) G_0(i\nu)). \quad (20)$$

In the last term in Eq.(20) we have added an exponential in order to regularize the sum over Matsubara frequencies correctly. This regularization affects only the first-order term in

g. We found that it is not advisable in general to carry out the frequency sum in Eq.(20) directly on the computer but to rewrite it as a contour integral in the complex plane and to evaluate it as an integral along the cut on the real frequency axis. One obtains in this way

$$V(\tilde{\phi}) = \frac{\omega_0^2}{2}(\tilde{\phi} + \langle \phi \rangle)^2 - \frac{2}{\pi} \int_{-\infty}^{+\infty} d\omega f(\omega) \left\{ \arctan \left(\frac{g\tilde{\phi}\Im G_0(\omega+i\eta)}{1-g\tilde{\phi}\Re G_0(\omega+i\eta)} \right) - \pi\theta(g\tilde{\phi}\Re G_0(\omega+i\eta) - 1) \text{sign}(\tilde{\phi}) \right\}. \quad (21)$$

Here f denotes the Fermi function, \Re and \Im real and imaginary parts, respectively, and θ and sign the theta- and sign-functions, respectively. In the case of the Lorentz model the integral in Eq.(21) can be performed analytically and one obtains at zero temperature:

$$V(\tilde{\phi}) = \frac{1}{2}\omega_0^2(\tilde{\phi} + \langle \phi \rangle)^2 - 1/\pi[-2g\tilde{\phi}\arctan\left(\frac{t}{g\tilde{\phi}}\right) + t\log\left(\frac{t^2}{(g\tilde{\phi})^2 + t^2}\right) + \pi(g\tilde{\phi})\text{sign}(\tilde{\phi}) - \pi g\tilde{\phi}]. \quad (22)$$

A conventional way to calculate corrections to the above local terms is to use a gradient expansion²⁴. One expands then the propagators in powers of frequencies $\omega_1 \dots \omega_n$ and rewrites these powers in terms of time derivatives acting on the field $\tilde{\phi}$. Such a procedure is, however, not possible in our case because of the appearance of nonanalytic terms. To see this let us first look at the lowest-order term $n = 2$:

$$X_2 = -\frac{g^2}{2}Tr(G_0\tilde{\phi}G_0\tilde{\phi}) = -\frac{g^2}{2}\sum_n \tilde{\phi}(n)\Pi(i\omega_n)\tilde{\phi}(-n), \quad (23)$$

with

$$\Pi(i\omega_n) = 2\sum_m G_0(i\omega_m)G_0(i\omega_m + i\omega_n). \quad (24)$$

Using the spectral representation

$$G_0(i\omega_n) = \int d\epsilon \frac{\rho(\epsilon)}{i\omega_n - \epsilon} \quad (25)$$

and carrying out the integrations one obtains at small frequencies and low temperatures and also disregarding a constant term

$$\Pi(i\omega_n) = 2\pi\rho^2(0)\beta|\omega_n|, \quad (26)$$

where $\rho(0)$ is the spectral function at the chemical potential $\mu = 0$. Considering X_2 as an self-energy contribution to the unperturbed phonon propagator in Eq.(12) and performing the analytic continuation $|\omega_n| \rightarrow \sqrt{-(\omega + i\eta)^2} \rightarrow -i\omega$, one recognizes that X_2 describes the damping of phonons which is smaller than the phonon frequency ω_0 by the Migdal paramter γ . Eq.(26) shows, however, that such a damping term produces a nonanalytic dependency in S_{ph} on Matsubara frequencies. This rules out a straightforward application of the usual gradient expansion. Such an expansion would correspond to a Taylor expansion of Π in powers of $i\omega_n$. Since Π has to be even in $i\omega_n$ its linear term would vanish and the leading term would be of second order in $i\omega_n$ in disagreement with the exact result Eq.(26). To overcome this problem we will use in the following a modified version of a gradient expansion which is able to give the leading non-local corrections to the local term also in our case.

In leading order in γ or, equivalently, in the local approximation, we assumed that the electrons in the general n -th order term X_n given in Eq.(19) interact elastically with the phonons. The first correction to that obviously is obtained by considering in this diagram 2 vertices where the electrons are inelastically and $n-2$ vertices where the electrons are elastically scattered. The case of one vertex with inelastic scattering is not possible due to the conservation of Matsubara frequencies. The analytic expression for X_n is, taking the above processes into account,

$$X_n^{(2)} = -\frac{g^n}{n} \sum_{i \neq j} \sum_{\substack{\omega_1 \dots \omega_n \\ \nu}} T \int_0^\beta d\tau e^{i(\omega_1 + \dots + \omega_n)\tau} \tilde{\phi}(\omega_1) G_0(i\nu) \tilde{\phi}(\omega_2) G_0(i\nu) \dots \tilde{\phi}(\omega_i) G_0(i\nu + \omega_i) \tilde{\phi}(\omega_{i+1}) G_0(i\nu + \omega_i) \dots \tilde{\phi}(\omega_j) G_0(i\nu) \tilde{\phi}(\omega_{j+1}) G_0(i\nu) \dots \tilde{\phi}(\omega_n) G_0(i\nu). \quad (27)$$

i and j are the two vertices where inelastic scattering occurs. A factor $1/2$ has also been introduced in order not to overcount the contributions. However, this factor is compensated by the spin factor 2. The superscript 2 at X indicates that all processes are taken into account where inelastic scattering takes place at two vertices.

The sums over $\omega_1 \dots \omega_i$ and $\omega_{j+1} \dots \omega_n$ can be carried out in Eq.(27) yielding

$$X_n^{(2)} = -g^2/n \sum_{i \neq j} \sum_{\omega_i, \omega_j} T \int_0^\beta d\tau e^{i(\omega_i + \omega_j)\tau} \tilde{\phi}(\omega_i) \tilde{\phi}(\omega_j) \tilde{G}^{(n-j+i-1)}(i\nu) \tilde{G}^{(j-i-1)}. \quad (28)$$

\tilde{G} is defined by

$$\tilde{G}^{-1}(i\nu) = G_0^{-1}(i\nu) - g\tilde{\phi}(\tau). \quad (29)$$

$\tilde{G}^{(i)}$ denotes \tilde{G} , calculated in i -th order in the coupling constant g , i.e.,

$$\tilde{G}^{(i)}(i\nu) = (g\tilde{\phi}(\tau))^i G_0^{i+1}(i\nu). \quad (30)$$

Keeping only the term $i = 1$ in Eq.(28) is equivalent to omitting the prefactor $1/n$. Moreover, the sum over $j \neq i$ can easily be carried out yielding

$$X_n^{(2)} = -g^2 \sum_{\omega_1, \omega_2} \int_0^\beta d\tau e^{i(\omega_1 + \omega_2)\tau} \tilde{\phi}(\omega_1) \tilde{\phi}(\omega_2) T \sum_{\nu} \tilde{G}(i\nu) \tilde{G}(i\nu + i\omega_1), \quad (31)$$

where all terms of order $n - 2$ have to be taken into account in the product of the two Green's functions \tilde{G} . Performing the sum over ν in Eq.(31), using the spectral function $\tilde{\rho}$ of \tilde{G} , and also summing over ω_2 we obtain

$$X_n^{(2)} = -g^2 T \int_0^\beta d\tau d\tau' \left(\sum_{\omega_1} e^{i\omega_1(\tau - \tau')} |\omega_1| \right) \tilde{\phi}(\tau) \tilde{\phi}(\tau') F[\phi(\tau)], \quad (32)$$

with

$$F[\phi] = -\pi \tilde{\rho}^2(0). \quad (33)$$

$\tilde{\rho}$ is the spectral function of \tilde{G} which also depends on $\tilde{\phi}(\tau)$. Splitting the sum over ω_1 in Eq.(32) into positive and negative parts, representing ω_1 as a time derivative which then is subjected to a partial integration, and finally performing the sums over ω_1 and n we obtain for the leading term of the nonlocal part $V_{NL}(\tilde{\phi})$ of S_{ph} the following expression

$$V_{NL}(\tilde{\phi}) = \frac{g^2}{2} T^2 \int_0^\beta d\tau d\tau' \frac{\sin(2\pi T(\tau - \tau'))}{1 - \cos(2\pi T(\tau - \tau'))} \tilde{\phi}(\tau) \frac{\partial \tilde{\phi}(\tau')}{\partial \tau'} G[\tilde{\phi}(\tau), \tilde{\phi}(\tau')], \quad (34)$$

with

$$G[\tilde{\phi}(\tau), \tilde{\phi}(\tau')] = F[\tilde{\phi}(\tau)] + F[\tilde{\phi}(\tau')] - \frac{\partial F}{\partial \tilde{\phi}(\tau')} \cdot \tilde{\phi}(\tau'). \quad (35)$$

V_{NL} vanishes for a constant field $\tilde{\phi}$ so it represents a nonlocal correction to the local potential V . V_{NL} , on the other hand, still depends on two arguments τ and τ' which would not occur if a usual gradient expansion would be applicable. This feature is caused by the nonanalyticity of Π in Eq.(26): $|\omega_n|$ cannot be represented just by one derivative but only by infinite many of them causing the appearance of two arguments τ and τ' in Eq.(34). We also would like to point out that the expression Eq.(34) is very similar to that derived by Hamann²⁵ for the Hubbard model using asymptotic approximations for G_0 and avoiding a gradient expansion.

IV. THE LOCAL ELECTRONIC GREEN'S FUNCTION G_{LOC}

The exact local Green's function G_{loc} of the impurity problem can be obtained from the relation

$$G_{loc}(\tau - \tau') = \frac{\delta \log Z}{\delta G_0^{-1}(\tau - \tau')}. \quad (36)$$

Carrying out the functional derivative we obtain

$$G_{loc}(\tau - \tau') = \int D\tilde{\phi} (G_0^{-1}(\tau_1 - \tau_2) - g\tilde{\phi}(\tau_1)\delta(\tau_1 - \tau_2))_{\tau-\tau'}^{-1} e^{S_{ph}}/Z. \quad (37)$$

S_{ph} is given by Eq.(12) where the $Tr \log$ term has been approximated by the local and nonlocal potentials V and V_{NL} . The simplest approximation for the functional integral in Eq.(37) is obtained by considering $\tilde{\phi}$ as a classical field and assuming the mass of the atoms to be infinite. The kinetic energy of the atoms as well as the nonlocal part in S_{ph} drops then out and the functional integral becomes a usual integral. As a result we have

$$G_{loc}(\tau - \tau') = \int_{\infty}^{\infty} d\tilde{\phi} (G_0^{-1} - g\tilde{\phi})_{\tau-\tau'}^{-1} e^{-\beta V(\tilde{\phi})}/Z. \quad (38)$$

Eq.(38) says that G_{loc} is to be calculated for a general displacement $\tilde{\phi}$ and then the result is averaged over all displacements using a Boltzmann factor. In this approximation the electrons no longer form a Fermi liquid and there is no quasiparticle peak in the electron

Green's function. For a finite mass of the atoms such an approach is valid if $T \gg \omega_0$. The dynamical mean field approximation on a Bethe lattice amounts then to solve Eqs. (9), (20) and (38) self-consistently^{21,22}.

A general approximation scheme for path integrals valid especially at low temperatures is based on expansions around stationary paths of the action S_{eff} . These paths are solutions of the equation

$$\frac{\delta S_{eff}[\tilde{\phi}]}{\delta \tilde{\phi}(\tau)} = 0. \quad (39)$$

We will see that Eq.(39) has in general 3 solutions, two of them being constant in time and one depending on time. The surroundings of these solutions will yield the major contributions to G_{loc} .

A. Contributions to G_{loc} from small fluctuations

Time-independent solutions of Eq.(39) satisfy also the equation

$$\frac{\delta V[\tilde{\phi}]}{\delta \tilde{\phi}} = 0. \quad (40)$$

Taking stability considerations into account the relevant solutions of Eq.(40) correspond to the minima of V which will be denoted by $\tilde{\phi}_\alpha$, where α counts different minima. We expand now the field $\tilde{\phi}$ around each minimum $\tilde{\phi}_\alpha$:

$$\tilde{\phi} = \tilde{\phi}_\alpha + \phi'_\alpha. \quad (41)$$

Inserting Eq.(41) into S_{ph} we write

$$S_{ph}(\tilde{\phi}_\alpha + \phi'_\alpha) = S_{ph,\alpha}^{(0)} + S'_{ph,\alpha}, \quad (42)$$

where $S_{ph,\alpha}^{(0)}$ contains the kinetic energy of the atoms and the quadratic terms in ϕ'_α of V . $S'_{ph,\alpha}$ is due to the anharmonic part of V around the minimum α and the nonlocal part V_{NL} . Expanding the inverse in Eq.(37) in powers of ϕ'_α as well as the exponential in powers of $S'_{ph,\alpha}$ one obtains path integrals over the displacement field containing an arbitrary number of

powers in ϕ'_α . Since the action in these path integrals is $S_{ph,\alpha}^{(0)}$ Wick's theorem can be applied. Contributions to G_{loc} from the minimum α , called G_α in the following, are thus obtained in terms of usual diagrams due to the electron-phonon and anharmonic interactions. As usual it is sufficient to consider self-energy diagrams Σ_α to G_α . G_α and Σ_α are related by

$$G_\alpha^{-1} = G_{0,\alpha}^{-1} - \Sigma_\alpha, \quad (43)$$

where $G_{0,\alpha}$ is the shifted unperturbed Green's function defined by

$$G_{0,\alpha}^{-1} = G_0^{-1} - g\tilde{\phi}_\alpha. \quad (44)$$

Fig. 1 shows the lowest-order skeleton diagrams for Σ_α which are of second (diagram (a)) and of fourth order (diagram (b)) in g . All uncrossed diagrams are taken into account by diagram (a), whereas diagram (b) represents the lowest order vertex correction to (a). In conventional treatments of the electron-phonon coupling it is argued that diagram (b) is smaller by the factor $\lambda\omega_0/t$ compared to the diagram (a). Whether this is true also in our case is not apriori clear because Migdal's theorem relies heavily on properties of momentum integrals and phase space arguments for which there is no analogue in our case.

In order to judge the convergence of the perturbation expansion around $\tilde{\phi}_\alpha$ we have calculated diagrams (a) and (b). One obtains

$$\Sigma_\alpha^{(a)}(i\omega_n) = -\frac{g^2}{2\omega_0}b(\omega_0)G_\alpha(i\omega_n + \omega_0) + \frac{g^2}{2\omega_0}b(-\omega_0)G_\alpha(i\omega_n - \omega_0) + g^2 \int d\epsilon \rho_\alpha(\epsilon) f(\epsilon) \frac{1}{(\epsilon - i\omega_n)^2 - \omega_0^2}, \quad (45)$$

where $\rho_\alpha(\epsilon)$ is the spectral function of G_α and b is the Bose distribution function.

$\Sigma_\alpha^{(b)}$ is given by

$$\begin{aligned} \Sigma_\alpha^{(b)} = & \sum_{s,t=\pm 1} (-1)^{(s+t+2)/2} \frac{g^4}{4\omega_0^2} \int d\epsilon d\epsilon' d\epsilon'' \frac{\rho_\alpha(\epsilon)\rho_\alpha(\epsilon')\rho_\alpha(\epsilon'')}{(-\epsilon + i\omega_n + s\omega_0)(-\epsilon'' + i\omega_n + t\omega_0)} \\ & \left(\frac{A(\epsilon', s, t)}{i\omega_n + s\omega_0 + t\omega_0 - \epsilon'} + \frac{B(\epsilon, \epsilon', t)}{\epsilon - \epsilon' + t\omega_0} + \frac{C(\epsilon', \epsilon'', s)}{\epsilon'' + s\omega_0 - \epsilon'} + \frac{D(\epsilon, \epsilon', \epsilon'')}{\epsilon - i\omega_n + \epsilon'' - \epsilon'} \right), \end{aligned} \quad (46)$$

with

$$A(\epsilon', s, t) = (b(t\omega_0) + f(\epsilon'))(b(s\omega_0) + f(\epsilon' - t\omega_0)), \quad (47)$$

$$B(\epsilon, \epsilon', t) = (b(t\omega_0) + f(\epsilon'))(f(\epsilon) - f(-t\omega_0 + \epsilon')), \quad (48)$$

$$C(\epsilon', \epsilon'', s) = (f(\epsilon'') - f(\epsilon'))(b(s\omega_0) - b(\epsilon' - \epsilon'')), \quad (49)$$

$$D(\epsilon, \epsilon', \epsilon'') = (f(\epsilon'') - f(\epsilon'))(f(\epsilon) + b(\epsilon' - \epsilon'')). \quad (50)$$

Figs. 2 and 3 present numerical results for the imaginary parts of diagrams (a) (solid lines) and (b) (dashed lines) as a function of frequency. In Fig. 2 (3) we used the parameters $\lambda = 1.0$ (1.375), $\omega_0 = 0.1$, and $T = 0.01$, where all energies are expressed in units of t . G_α has been calculated using the self-consistently determined function G_0 described in the next section. The potential V develops a double well around $\lambda = 1.2$ so that Figs. 2 and 3 correspond to the cases with one and two minima, respectively. If Migdal's theorem would hold diagram (b) should be smaller by one order of magnitude compared to diagram (a). The Figures show that this is approximately the case which validates the employed perturbation expansion.

The above result is nontrivial, especially, at large couplings when the double well has been formed. As illustrated in the next section the main weight of G_0 resides in this case in a narrow, central component at zero frequency. The characteristic energy of G_0 thus may be low and comparable with ω_0 making a simple perturbation theory of Σ_α in terms of $G_{0,\alpha}$ impossible. On the other hand, G_α consists at large couplings of a broad peak of width $\sim t$ around $\tilde{\phi}_\alpha$. The effective expansion parameter for an expansion of Σ in terms of G_α can easily be determined for large couplings where one can assume that $ImG_\alpha(\omega)$ is only non-zero for $\omega < -\omega_0$. Eqs.(45) and (46) reduce then at $T = 0$ to

$$\Sigma_\alpha^{(a)} \rightarrow \frac{g^2}{2\omega_0} G_\alpha(\omega + i\eta + \omega_0), \quad (51)$$

$$\Sigma_\alpha^{(b)} \rightarrow \frac{g^4}{4\omega_0^2} G_\alpha^2(\omega + i\eta + \omega_0) G_\alpha(\omega + i\eta + 2\omega_0). \quad (52)$$

The ratio $\Sigma_\alpha^{(b)}/\Sigma_\alpha^{(a)}$ is thus $\sim g^2/\omega_0 t^2 = \lambda\omega_0/t$ which is in agreement with the above numerical calculations. Nonvanishing potential minima at $\tilde{\phi}_\alpha$ signalize the appearance of nonadiabatic effects: at large couplings electrons occupy predominantly ionic configurations with zero or 2 electrons at the atom. In each case the lattice relaxes to a non-vanishing value similar as in the anti-adiabatic case. As shown above, the perturbation expansions around the potential minima are, however, still controlled by the Migdal parameter $\lambda\omega_0/t$.

According to our previous discussion the nonlocal potential V_{NL} is smaller by the Migdal parameter γ compared to the local potential. To make this more quantitative we have calculated the imaginary-part of the self-energy of V_{NL} for a harmonic phonon with frequency ω_0 for a fixed, but general field value $\tilde{\phi}$. The result is shown in Fig. 4 for the two coupling strengths used in Figs. 2 and 3 using again the self-consistent function G_0 . The position of the potential minima are indicated by arrows. One concludes from Fig. 4 that the damping of the oscillations around the potential minima is small enough in each case so that one may neglect it. Finally, we have neglected anharmonic effects. This is an excellent approximation at small and large couplings λ but not for intermediate couplings where the double well forms. A simple prescription to take anharmonic effects into account which is based on the exact atomic eigenfunctions in the potential V will be described in the next section.

B. Instanton contribution to G_{loc}

At half-filling the potential V is symmetric with respect to $\tilde{\phi} = 0$. If V has two minima they are equivalent and the potential barrier between them is finite. The appearance of tunnelling processes between the minima manifests itself in a third, time-dependent solution of Eq.(39)²⁶. This instanton solution passes from one minimum to the other as function of τ and is relevant at low temperatures where this passage occurs within the interval $[0, \beta]$. One instanton solution creates, however, a whole family of approximate solutions of Eq.(39): The passage from one to the other minimum can take place everywhere in the interval

$[0, \beta]$; furthermore, multi-instanton configuration are also approximate solutions of Eq (39) and must be taken into account. For each instanton configuration we expand the inverse in Eq.(39) in powers of $\tilde{\phi}$ and sum then over all configurations using the rules derived in Ref.²⁶. The first-order term in $\tilde{\phi}$ vanishes by symmetry. The second-order self-energy can be represented by the diagram a) in Fig. 1 where the phonon propagator is to be replaced by the instanton propagator

$$D_I(i\omega_n) = \tilde{\phi}_1^2 \frac{1 - e^{-\Delta E \beta}}{1 + e^{-\Delta E \beta}} \cdot \frac{2\Delta E}{\omega_n^2 + (\Delta E)^2}. \quad (53)$$

$\tilde{\phi}_1^2$ is the squared field value of one of the two minima. If V_{NL} can be neglected ΔE denotes the tunnelling frequency of one atom through the potential V between the minima. In general, ΔE contains an additional exponential factor with the action due to V_{NL} along one instanton in the exponent. D_I has the form of a phonon propagator with the phonon frequency replaced by ΔE and an additional prefactor $\sim \Delta E/T$ at temperatures large compared to the tunnelling frequency.

The second-order instanton contribution to the self-energy becomes

$$\begin{aligned} \Sigma_I(i\omega_n) = & g^2 \tilde{\phi}_1^2 \frac{1 - e^{-\Delta E \beta}}{1 + e^{-\Delta E \beta}} \left(-b(\Delta E) G_0(i\omega_n + \Delta E) + b(-\Delta E) G_0(i\omega_n - \Delta E) \right. \\ & \left. + \frac{g^2}{\omega_0} \int d\epsilon \rho(\epsilon) f(\epsilon) \frac{\Delta E}{(\epsilon - i\omega_n)^2 - (\Delta E)^2} \right), \end{aligned} \quad (54)$$

where $\rho(\epsilon)$ is the spectral function of $G_0(\epsilon)$. In the limit $\Delta E \rightarrow 0$ Σ_I approaches $\tilde{\phi}_1^2 G_0(i\omega_0)$. Inserting this into Eq.(37) one finds the contribution

$$G'_{loc} = \frac{1}{2} \left(\frac{1}{G_0^{-1} + g\tilde{\phi}_1} + \frac{1}{G_0^{-1} - g\tilde{\phi}_1} \right), \quad (55)$$

to G_{loc} . G'_{loc} is due to the integration over the paths along the two minima of V which are also included in Σ_I . This contribution has already been taken into account when integrating over paths near the first two stationary path at $\tilde{\phi}_\alpha$ and thus should be subtracted again. The pure instanton contribution to G_{loc} is thus given in lowest-order perturbation theory by

$$G_I = \frac{1}{G_0^{-1} - \Sigma_I} - G'_{loc}. \quad (56)$$

After the analytic continuation the imaginary part of Σ_I deviates from $\tilde{\phi}_1^2 G_0(\omega + i\eta)$ only at small frequencies $\omega \sim \Delta E$ where it rapidly decreases and approaches zero at zero temperature assuming that the characteristic energy scale t^* of G_0 is larger than ΔE . Thus the instanton contribution to G_{loc} provides the finite value of G_{loc} of Fermi liquid theory at $\mu = 0$ in form of a Kondo resonance peak with an exponentially small width determined by ΔE .

The expansion of the denominator on the right-hand side of Eq.(37) in powers of $g\tilde{\phi}$ seems to be problematic for instanton field configurations because in this case $g\tilde{\phi}$ can in general not be considered as small compared to G_0^{-1} . This is also true if the perturbation series is resummed by means of the self-energy Σ_I and if the latter is approximated by its lowest-order expression in g . In the remainder of this subsection we will show that G_I can be obtained in closed form without using an expansion of the denominator in Eq.(37). The only assumption is that the instanton gas is dilute, i.e., that self-energy effects for the tunnel modes can be neglected.

Let us first disregard the nonlocal part V_{NL} in the atomic potential. The Hamiltonian for the impurity atom is then hermitean and can be diagonalized yielding two low-lying states which are split by tunnelling processes. Disregarding small oscillations around the extremal paths the evaluation of the path integral by instanton solutions corresponds to the solution of the Schroedinger equation for the two lowest-lying states of the Hamiltonian. Thus the instanton part of the electron Green's function, G_I , can also be obtained from an effective two-level model with the Hamiltonian

$$H_I = \frac{\Delta E}{2}(X^{11} - X^{00}). \quad (57)$$

X^{11} and X^{00} are Hubbard operators defined as the projection operators $|1><1|$ and $|0><0|$, respectively, where $|0>$, $|1>$ are the two lowest states of the atomic Hamiltonian and ΔE their splitting. The field variable $\tilde{\phi}$ becomes

$$\tilde{\phi} = \tilde{\phi}_0(X^{01} + X^{10}), \quad (58)$$

where $\tilde{\phi}_0$ is the matrix element $\langle 0|\tilde{\phi}|1 \rangle$ which can be identified with the previous $\tilde{\phi}_1$ in a good approximation. The nondiagonal Hubbard operators X^{01} and X^{10} are given by $|0\rangle\langle 1|$ and $|1\rangle\langle 0|$, respectively. The (imaginary) time evolution of the nondiagonal operators due to H_I is

$$X^{01}(\tau) = e^{-\Delta E \tau} X^{01}(0), \quad (59)$$

$$X^{10}(\tau) = e^{\Delta E \tau} X^{10}(0). \quad (60)$$

Using Eqs.(59) and (60) the displacement Green's function $D_I(i\omega_n)$ can be calculated in a straightforward way and yields exactly the previous expression Eq.(53). Taking also V_{NL} into account changes the extremal instanton configurations. However, in the dilute instanton approximation, only the action along the extremal path enters. This means that ΔE acquires a different meaning in the effective two-level model but otherwise there is no change.

In the following it is convenient to use a description based on a Hamiltonian and not on a Lagrangian. To this end we consider the following effective Hamiltonian

$$\begin{aligned} H_{eff} = & \sum_{l\sigma} \tilde{\epsilon}_l a_{l\sigma}^\dagger a_{l\sigma} + \sum_{l\sigma} V_l (a_{l\sigma}^\dagger c_\sigma + c_\sigma^\dagger a_{l\sigma}) - \mu \sum_\sigma c_\sigma^\dagger c_\sigma \\ & + \frac{\Delta E}{2} (X^{11} - X^{00}) + g \phi_0 (X^{01} + X^{10}) \sum_\sigma c_\sigma^\dagger c_\sigma. \end{aligned} \quad (61)$$

The first three terms in H_{eff} represent an Anderson Hamiltonian for impurity electrons, described by $c_\sigma^\dagger, c_\sigma$, interacting with bath electrons, described by $a_{l\sigma}^\dagger, a_{l\sigma}$. As shown in Ref.¹⁴ elimination of the bath electrons allows to represent a general function G_0 in the effective impurity action. The fourth term represents H_I , and the last term the interaction between impurity electrons and the tunnel modes.

Neglecting self-energy effects in the tunnel modes the equation of motion for the composite operator $X^{pq}(\tau) c_\sigma(\tau)$ is, using H_{eff} ,

$$\frac{\partial}{\partial \tau} (X^{pq} c_\sigma) = \begin{cases} X^{00} \frac{\partial c_\sigma}{\partial \tau} & X^{01} (-\Delta E c_\sigma + \frac{\partial c_\sigma}{\partial \tau}) \\ X^{10} (\Delta E c_\sigma + \frac{\partial c_\sigma}{\partial \tau}) & X^{11} \frac{\partial c_\sigma}{\partial \tau} \end{cases}. \quad (62)$$

with $p, q = 0, 1$. The equations of motion for the operators c_σ and $a_{l\sigma}$ are

$$\frac{\partial c_\sigma}{\partial \tau} = \mu c_\sigma - g\phi_0(X^{01} + X^{10})c_\sigma - \sum_l V_l a_{l\sigma}, \quad (63)$$

$$\frac{\partial a_{l\sigma}}{\partial \tau} = -\tilde{\epsilon}a_{l\sigma} - V_l c_\sigma. \quad (64)$$

Inserting Eq.(64) into Eq.(63) yields

$$\int_0^\beta d\tau' \left[\delta(\tau - \tau') \left(-\frac{\partial}{\partial \tau'} + \mu \right) - \Lambda(\tau - \tau') \right] c_\sigma(\tau') = -g\phi_0(X^{01} + X^{10}), \quad (65)$$

with the function

$$\Lambda(\tau - \tau') = T \sum_{l,n} V_l^2 \frac{e^{-i\omega_n(\tau - \tau')}}{i\omega_n - \tilde{\epsilon}}. \quad (66)$$

Inserting Eq.(65) into Eq.(62) yields

$$\int_0^\beta d\tau' \left[\delta(\tau - \tau') \left(\frac{\partial}{\partial \tau'} - \mu \right) + \Lambda^{pq}(\tau - \tau') \right] X^{pq}(\tau') c_\sigma(\tau') = \sum_{p'q'} M_{pq,p'q'} X^{p'q'}(\tau) c_\sigma(\tau). \quad (67)$$

The only non-vanishing elements of M are

$$M_{00,01} = M_{01,00} = M_{10,11} = M_{11,10} = -g\phi_0, \quad (68)$$

$$M_{10,10} = -M_{01,01} = \Delta E. \quad (69)$$

We also used the definitions

$$\Lambda^{00}(\tau - \tau') = \Lambda^{11}(\tau - \tau') = \Lambda(\tau - \tau'), \quad (70)$$

$$\Lambda^{01}(\tau - \tau') = \Lambda(\tau - \tau') e^{-\Delta E(\tau - \tau')}, \quad (71)$$

$$\Lambda^{10}(\tau - \tau') = \Lambda(\tau - \tau') e^{\Delta E(\tau - \tau')}. \quad (72)$$

Let us now define the following Matsubara Green's functions

$$G(\frac{pq}{\tau - \tau'}) = -\langle T(X^{pq}(\tau) c_\sigma(\tau) c_\sigma^\dagger(\tau')) \rangle. \quad (73)$$

They satisfy the equation of motion

$$\int_0^\beta d\tau'' G_0^{-1} \left(\frac{pq}{\tau - \tau''} \right) G \left(\frac{pq}{\tau'' - \tau'} \right) + \sum_{p'q'} M_{pq,p'q'} G \left(\frac{p'q'}{\tau - \tau'} \right) = \delta(\tau - \tau') \langle X^{pq} \rangle, \quad (74)$$

with the definition

$$G_0^{-1} \left(\frac{pq}{\tau - \tau'} \right) = \delta(\tau - \tau') \left(-\frac{\partial}{\partial \tau''} + \mu \right) - \Lambda^{pq}(\tau - \tau'). \quad (75)$$

Comparing Eqs.(70) and (75) with Eqs.(14) and (15) of Ref.¹⁴ one finds that

$$G_0 \left(\frac{00}{\tau - \tau'} \right) = G_0 \left(\frac{11}{\tau - \tau'} \right) = G_0(\tau - \tau'). \quad (76)$$

Furthermore, one can easily verify that Eq.(75) yields

$$G_0 \left(\frac{10}{\tau - \tau'} \right) = G_0(\tau - \tau') e^{\Delta E(\tau - \tau')}, \quad (77)$$

$$G_0 \left(\frac{01}{\tau - \tau'} \right) = G_0(\tau - \tau') e^{-\Delta E(\tau - \tau')}. \quad (78)$$

Using these results and eliminating the non-diagonal Green's functions one finds that Eq.(74) is equivalent with the two equations

$$G \left(\frac{00}{\tau - \tau'} \right) = G_0(\tau - \tau') \langle X^{00} \rangle + g^2 \phi_0^2 \int_0^\beta d\tau'' d\tau''' G_0(\tau - \tau'') G_0(\tau'' - \tau''') e^{-\Delta E(\tau'' - \tau''')} G \left(\frac{00}{\tau''' - \tau'} \right), \quad (79)$$

$$G \left(\frac{11}{\tau - \tau'} \right) = G_0(\tau - \tau') \langle X^{11} \rangle + g^2 \phi_0^2 \int_0^\beta d\tau'' d\tau''' G_0(\tau - \tau'') G_0(\tau'' - \tau''') e^{\Delta E(\tau'' - \tau''')} G \left(\frac{00}{\tau''' - \tau'} \right). \quad (80)$$

Eqs.(79) and (80) can easily be solved in ω -space. One obtains then an explicit expression for the wanted Green's function

$$G(i\omega_n) = G \left(\frac{00}{i\omega_n} \right) + G \left(\frac{11}{i\omega_n} \right). \quad (81)$$

From G one obtains the following expression for the self-energy Σ_I :

$$\Sigma_I(i\omega_n) = \frac{< X^{00} > \Pi^{(1)}(i\omega_n) + < X^{11} > \Pi^{(2)}(i\omega_n) - G_0(i\omega_n)\Pi^{(1)}(i\omega_n)\Pi^{(2)}(i\omega_n)}{1 - G_0(i\omega_n)(< X^{00} > \Pi^{(2)}(i\omega_n) + < X^{11} > \Pi^{(1)}(i\omega_n))}, \quad (82)$$

with

$$\Pi^{(1,2)}(i\omega_n) = g^2 \phi_0^2 T \sum_m G_0(i\omega_m) \frac{e^{\mp \Delta E \beta} - 1}{i\omega_n - i\omega_m \mp \Delta E}, \quad (83)$$

where the upper (lower) signs in front of ΔE refer to the superscripts 1 (2). In the weak-coupling limit $g \ll 1$, but also in the high-temperature limit $\Delta E \beta \ll 1$, Eqs.(82) and (83) reduce exactly to the previous result Eq.(54). The same also holds at zero temperature where $< X^{00} > = 1$ and $< X^{11} > = 0$. Eqs.(54) and (82) have, for a finite ΔE , also the same low temperature limit which is a rather astonishing result.

Taking all together the local Green's function has been obtained in general as a sum of three contributions

$$G_{loc} = \frac{Z_1}{Z} G_1 + \frac{Z_2}{Z} G_2 + G_I. \quad (84)$$

Z_α is the contribution of the minimum α to the partition function Z . At small couplings V has only one minimum at $\tilde{\phi} = 0$. There exists then only the first term in Eq.(84) with $Z_1/Z = 1$ and the perturbation theory can be carried out in powers of $\tilde{\phi}$ as usual. Beyond a critical coupling strength V develops two minima. The perturbation theory must then be performed around each minimum separately yielding the first two terms in Eq.(58). There are in addition tunnelling processes between the two minima causing the third term in Eq.(84). The appearance of the prefactors Z_α/Z in Eq.(84) is due to the fact that the use of the linked cluster theorem in the expansion around α cancels the contribution Z_α . The definition Eq.(37) of G_{loc} implies then the above prefactors. The use of the linked cluster theorem in calculating G_I means that there is no prefactor in front of G_I in Eq.(84). In general $Z = Z_1 + Z_2 + Z_I$ where Z_I is the instanton contribution to G_{loc} . A convenient way to determine Z_I is to apply the sum rule to Eq.(84). In practice Z_I is small compared to Z so that $Z_1/Z = Z_2/Z = 1/2$ can be used in a very good approximation.

V. NUMERICAL RESULTS

In this section we discuss the results obtained by solving numerically the set of dynamical mean-field equations on the Bethe lattice. $\langle \phi \rangle$ was determined from Eq.(15) from the outset. Then we proceeded in an iterative way, starting with an educated guess for G_0 . The effective potential $V(\tilde{\phi})$ was then calculated from Eq.(21). The calculation of the local Green's function G_{loc} , given by Eq.(84), amounted to calculating the self-energies Σ_α and Σ_I . To account also for anharmonic effects we determined the stationary solutions of the Schrödinger equation for one atom in the potential V :

$$\frac{\partial^2 \psi_r(\tilde{\phi})}{\partial \tilde{\phi}^2} + 2[E_r - V(\tilde{\phi})]\psi_r(\tilde{\phi}) = 0. \quad (85)$$

r labels the different states with energy E_r and eigenfunction $\psi_r(\tilde{\phi})$. In the weak-coupling case, where V has only one minimum, we obtained the phonon propagator D using the exact energies and eigenstates,

$$D(i\omega_n) = \frac{1}{Z_{ph}} \sum_{r \neq s} e^{-\beta E_s} \frac{|\langle s|\tilde{\phi}|r\rangle|^2 (1 - e^{-\beta \Omega_{rs}})}{i\omega_n - \Omega_{rs}}, \quad (86)$$

with $\Omega_{rs} = E_r - E_s$ and $Z_{ph} = \sum_r e^{-\beta E_r}$. Only the first term in Eq.(84) is present and the corresponding self-energy is calculated from the diagram in Fig.1a) using Eq.(86) for the wavy line. As a result anharmonic effects were fully taken into account whereas higher-order skeleton diagrams and also V_{NL} can be neglected as shown in the previous section.

In the strong-coupling case V exhibits two minima. We treated the two lowest levels as a tunnel system and omitted the transitions between them in the phonon propagator Eq.(86). Furthermore, the remaining transitions in Eq.(86) can be ascribed either to the left or the right well because at least one wave function involved in the transition is localized. We found it most convenient to accomplish this splitting of D into left and right parts by dividing the matrix element $\langle s|\tilde{\phi}|r\rangle$ into contributions with $\tilde{\phi} > 0$ and $\tilde{\phi} < 0$ using also appropriate normalization factors. The self-energies $\Sigma_\alpha, \alpha = 1, 2$, were then calculated using again the diagram in Fig.1 (a) with the split phonon propagator as wavy line. Our procedure becomes

exact at large couplings and also provides a very smooth transition to the one-well case. Finally G_I was determined from Eq.(82). Since Eq.(82) approaches the simpler expression Eq.(52) in several limiting cases we found it sufficient to use Eq.(52) and also to neglect V_{NL} in calculating ΔE . Having obtained G_{loc} we determined a new G_0 from Eq.(9) and started a new cycle until convergency was reached.

A. Atomic properties

Fig. 5 shows the self-consistent potential V (in unit of the hopping t) as a function of the dimensionless phonon field $\xi = \tilde{\phi}\omega_0/t^{1/2}$ for $T = 0.1\omega_0 = 0.01t$. The dotted line corresponds to $\lambda = 0.5$, i.e., the weak-coupling case where V exhibits one minimum. The dashed curve refers to $\lambda = 1.2$ and corresponds to the case where the potential is very flat around $\xi \sim 0$ and the double well structure has just been formed. The double well becomes more and more pronounced with increasing λ as shown by the dot-dashed and solid lines. The dotted line in Fig. 6 shows the position of the potential minimum $R = \tilde{\phi}_1\omega_0/t^{1/2}$ as a function of λ for $T = 0.1\omega_0 = 0.01t$. The circles are calculated values which have been joined smoothly by the dotted curve. The Figure illustrates how rapidly R increases above the threshold value $\lambda_c \sim 1.15$. At large λ 's R approaches the curve $\sqrt{\lambda}$ shown in Fig. 6 as a solid line. The squares in Fig. 7, joined smoothly by a dashed line, represent the difference $(V_{max} - V_{min})/10$ in units of t as a function of λ . V_{max} and V_{min} are the values $V(0)$ and the minimum value of V , respectively. $V_{max} - V_{min}$ approaches at large λ the curve $\lambda/2$. The filled circles in Fig. 7 describe the energy difference Ω_{10} between the two lowest eigenvalues, i.e., a phonon frequency. This frequency is at $\lambda = 0$ equal to the bare phonon frequency $\omega_0 = 0.1t$. It softens with increasing λ and tends to a very small value when the double well has been formed. This “soft” phonon does not produce a structural phase transition for $\lambda > \lambda_c$ but switches over smoothly to the tunnel mode connecting the two potential minima. The corresponding frequency is practical zero on the energy scale of Fig. 7. The empty circles in Fig. 7 describe the excitation energy Ω_{20} . At $\lambda = 0$ it is equal

to $2\omega_0$, softens appreciably with increasing λ up to the critical value λ_c , and then recovers approaching ω_0 from below at large λ 's. Fig. 8 depicts three curves for the probability function $P(\xi)$ to find an atom at a distance ξ as a function of ξ . P shows for $\lambda = 0.5$ a one-peak structure which broadens and finally splits into two peaks with increasing λ . Finally, Fig. 9 shows the electron-phonon correlation function $C_0 = -g/t < \tilde{\phi}n >$ versus λ for $T = 0.1\omega_0 = 0.01t$. In the weak-coupling limit C_0 is very small which means that the atomic displacements are rather independent from electronic fluctuations and depend only on the average electronic density. This changes dramatically for $\lambda > \lambda_c$ where the atomic displacement depend strongly on the momentary electronic occupation of the atomic site.

The interpretation of the above results is rather straightforward. In the weak-coupling case, for instance at $\lambda = 0.5$, the atoms are according to their probability distribution function located mainly near $\xi \sim 0$ and have only a small mean square displacement from this position. From Eq.(9) follows that the charge fluctuations around the average value $n = 1$ are then also small. This is the situation corresponding to the description of a metal in the Migdal approximation: The electrons hop very often between sites during one atomic oscillation. As a result the atoms oscillate around their unperturbed equilibrium positions with only slightly changed frequencies. With increasing λ the potential energy of the electrons becomes more and more important compared to their kinetic energies and the electrons prefer to stay in doubly occupied sites. Since the average occupation of one site is forced to be one this means that each site is occupied for long times either with two or with zero electrons. The atoms adapt to each of this ionic configuration by relaxing either to the left or right potential minimum. If one assumes that the atoms have enough time to relax completely to the static equilibrium for each ionic configuration R is given by $\sqrt{\lambda}$. The solid line in Fig. 6 shows indeed that R approaches $\sqrt{\lambda}$ at large λ 's. Using a similar consideration $V_{max} - V_{min}$ should approach the curve $\lambda/2$, which is in agreement with Fig. 7. Finally, one expects that at large couplings the atoms oscillate more or less with the unperturbed frequency around the new equilibrium positions for each ionic configuration. This conclusion is also supported by the curve for Ω_{20} in Fig. 7.

Our path integral method coincides with the usual Migdal-Eliashberg perturbation expansion in the weak-coupling limit. In the strong-coupling case our method resembles in several respects treatments based on the Lang-Firsov transformation^{11,12}. One common feature is that the atoms acquire new equilibrium positions depending on the momentary electronic configuration. In the Lang-Firsov approach the new equilibrium values are given by $\xi = \pm\sqrt{\lambda}$. Fig. 6 shows for the Migdal parameter $\omega_0/t = 0.1$ that our expansion points $\pm R$ are near to these values for $\lambda \gg \lambda_c$. The perturbation expansion around these points, however, is ruled by different expansion parameters: In the Lang-Firsov case¹² by $1/\lambda$ and in our case by $\lambda \cdot \omega_0/t$. We also note that the appearance of expansion points different from zero signalizes the breakdown of the Migdal-Eliashberg expansion: In case of a double-well the information obtained by expansions around the minima cannot be retrieved by low-order diagrams of an expansion around the local maximum at $\xi = 0$. Our calculations imply that the validity of the Migdal-Eliashberg perturbation expansion is not solely governed by the condition $\lambda \cdot \omega_0/t \ll 1$, as often is assumed, but also by $\lambda \leq \lambda_c$, where λ_c lies around 1.2 for a small Migdal parameter ω_0/t . Based on the Lang-Firsov transformation the condition $\lambda \leq \lambda_c$ for the validity of the Migdal-Eliashberg expansion has also been stressed in Ref.¹¹.

B. Electronic properties at low temperatures

In this section we present numerical results for the electronic properties of the Holstein model. In the last section we have seen that the crossing from the weak to the strong-coupling regime is characterized by a drastic change in the effective atomic potential due to the appearance of anharmonic effects and the formation of a double well. These effects also cause typical features in the spectral properties of electrons. Fig. 10 shows the evolution of the spectral function $\rho(\omega) = -Im G_{loc}(\omega)/\pi$ with coupling strength λ as a function of frequency ω for a finite but low temperature $T = 0.1\omega_0 = 0.01t$. In case of the weak-coupling curve with $\lambda = 0.5$ $\rho(\omega)$ is somewhat broadened compared to the semicircular density of free electronic states. In the metallic state $\rho(0)$ should always be unrenormalized and equal

to $1/\pi$ at $T = 0$. Our value for $\rho(0)$ is slightly smaller than $1/\pi$ because of the finite temperature. For the next lower curve with $\lambda = 1.25$ the double well has already been formed. Nevertheless, $\rho(\omega)$ still consists of a broadened peak centered at $\omega = 0$. Atop of this broad structure is a narrow component caused also by the tunneling of atoms between the potential minima. With increasing λ the broad peak for ρ splits symmetrically into two peaks centered around $\pm\sqrt{\lambda}R$ with widths comparable to the width of the density of bare states. For $\lambda < 1.5$ the system is still in the metallic state, however, $\rho(0)$ is much smaller than the canonical value $1/\pi$. The reason for this is that the tunneling contribution mainly determines the value of $\rho(0)$. This contribution, however, is heavily quenched if the temperature is larger or comparable with the tunnelling energy ΔE . The latter becomes exponentially small at large λ 's. For our temperature $T = 0.1\omega_0$ the tunnel contribution to $\rho(\omega)$ is invisible small in plots like Fig. 10 when the two peaks already separate at around $\lambda \sim 1.5$. The interpretation of the curves in Fig. 10 is simple: For $\lambda < \sim 1.3$ charge fluctuations at a site around the average value 1 are small. For values for λ between ~ 1.3 and 1.5 the charge fluctuations become larger and larger and the electronic state at a site consists of a coherent superposition of a doubly and an unoccupied state. At $\lambda \sim 1.5$ the coherency is practically lost leading to an incoherent arrangement of doubly and unoccupied sites.

Fig. 11 shows the negative imaginary part of G_0 . For small λ 's this function resembles the density of bare states. With increasing λ it develops a strong central component which looks like a needle for $\lambda > 1.5$. At the same time spectral weight is shifted to the upper and lower ends of the spectrum which gradually transforms into an upper and lower subband. With increasing λ these subbands move away from the center and lose spectral weight. Fig. 12 shows the evolution of $-Im \Sigma(\omega)$ with λ as a function of ω for $T = 0.1\omega_0 = 0.01t$. For the values of λ on the left panel of this figure $-Im \Sigma$ is essentially proportional to the density of bare states except at small frequencies where it drops to small values reflecting the Fermi liquid ground state. The region of small values decreases with increasing λ due to the softening of the phonon and the appearance of the tunnel mode. For the larger values

for λ used in the right panel the spectral weight accumulates in a central component and two sidebands which move away from the center.

The low-frequency behavior of the real part of the self-energy can be characterized by an effective mass m^* defined by

$$m^*/m = 1 - \frac{d\text{Re}\Sigma(\omega)}{d\omega} \bigg|_{\omega=0}. \quad (87)$$

Figure 13 shows m^*/m as a function of λ for $T = 0.1\omega_0 = 0.01t$. At small λ the mass enhancement is given by $1 + \lambda/\pi$. Above $\lambda \sim 0.8$ m^* increases much stronger than linearly which announces localization and the transition to the insulating state. The metal-insulator transition can also be characterized by the frequency dependence of the ac conductivity $\sigma(\Omega)$ given by¹⁴

$$\sigma(\Omega) = \frac{2e^2t\pi}{\Omega} \int d\epsilon N(\epsilon) \int d\omega A(\omega, \epsilon) A(\omega + \Omega, \epsilon) (f(\omega) - f(\omega + \Omega)). \quad (88)$$

$A(\omega, \epsilon) = -\text{Im } G(\omega, \epsilon)/\pi$ is the one particle spectral function of the lattice Green's function. $\sigma(\omega)$ is shown in Fig. 14 for four different values of λ . The large Drude peak seen for $\lambda = 1.2$ splits for $\lambda = 1.36$ into a small peak at $\omega = 0$ and a broader peak at a finite value of ω . Beyond $\lambda \sim 1.4$ the Drude peak has virtually vanished and all spectral weight has been accumulated in the broad peak caused by transitions between the two subbands.

Fig. 15 shows the frequency dependence of the spectral function $A(\omega, \epsilon)$ of the lattice Green's function at the Fermi surface $\epsilon = 0$. The thick solid line corresponding to $\lambda = 1.36$ exhibits the quasiparticle peak at $\omega = 0$ and a rather well developed two-peak structure of the incoherent background. The thin solid line represents the same spectral function calculated within the Migdal-Eliashberg perturbation expansion where the phonon field is expanded around $\tilde{\phi} = 0$. The same parameter has been used as well as the exact eigenstates in the potential V . The quasi-particle peak is in this case more pronounced and the incoherent background is structureless. Our path integral approach shows that the point $\tilde{\phi} = 0$ is an unstable extremal point in this case and that the two potential minima are stable extremal points suitable for expansions. This clearly means that the thin line in Fig. 15 is incorrect

and that the Migdal- Eliashberg expansion has broken down in spite of the small Migdal parameter $\gamma = 0.1$ used in this figure. For $\lambda = 2$ both the thick and thin dashed-dotted curves exhibit no longer visible quasiparticle peaks at $\omega = 0$. The Migdal-Eliashberg expansion, however, is unable to reproduce the two-peak structure of the incoherent background but instead shows a broad and structureless peak. Though a double well potential has been formed already for $\lambda = 1.25$ the two approaches give similar results in this case, mainly because the first excited state is above the barrier and the trajectories of the atom are rather delocalized. This means that for a Migdal parameter of 0.1 the Migdal-Eliashberg expansion breaks down for $\lambda \geq 1.25$.

C. Electronic properties at high temperatures

To complete the overview of the electronic properties we show here also results obtained in the limit $T \gg \omega_0$. This limit is equivalent to the limit $\omega_0 \rightarrow 0$ and corresponds to the case where the phonons behave like a quasi-static, classical field. G_{loc} can then be calculated from Eq.(38) and an explicit high-temperature expansion of Eq.(45) and (46) shows that the corrections are of the order $\lambda\omega_0/T$. On the other hand, the validity of our general quantum-mechanical approach requires $\lambda\omega_0/t \ll 1$ and $\lambda T/t \ll 1$. The first inequality follows from Eqs.(51) and (52), the second one by expanding Eqs.(45) and (46) at high temperatures after taking the limit $\omega_0 \rightarrow 0$.

The above expansion parameters suggest that the two approaches should yield similar results if $\omega_0 \ll T \ll t$. To check this we calculated $\rho(\omega)$ for $T = 2.0\omega_0 = 0.2t$. The results are shown in Figs. 16 and 17. For $\lambda = 0.5$ the above expansion parameters are small and the two corresponding curves indeed are practically coincident. This agrees with the observation that in the quantum-mechanical approach $Im \Sigma(\omega = 0)$ is already so large that the quasi-particle peak in the spectral function of the lattice Green's function has completely vanished. For $\lambda > 1.2$ similar double well potentials form in the two cases. In the quantum-mechanical treatment the instanton contribution can safely be neglected at

these high temperatures and thermally activated processes seem somewhat impeded by the level quantization compared to the classical case. As a result the splitting of the band into two subbands occurs more slowly in the classical, quasi-static case than in the quantum-mechanical case. For $\lambda = 4$. $\rho(\omega)$ shows in both cases well-split bands with a pseudo-gap in between where the density is finite but exponentially small. In Fig. 16 the shape of the two peaks resembles the bare density of the Bethe lattice whereas in Fig. 17 the shape is more Gaussian with well-developed tails into the pseudo-gap. The two Figures illustrate that the quantum-mechanical treatment approaches smoothly the classical case with infinite heavy atoms at high temperatures and agrees with the latter also quantitatively if all expansion parameters are small.

VI. CONCLUSIONS

We have studied the Holstein model in infinite dimensions at half-filling in the normal state. In contrast to recent semiclassical treatments we consider the atomic displacements as a quantized, dynamical field which enables us to recover Fermi liquid properties at low temperatures in the metallic state. Our approximation scheme is based on expansions of path integrals around extremal paths of the action. This method allows to treat arbitrary strengths of the coupling constant λ on the same footing. For each stationary path a Migdal-Eliashberg-like expansion is generated which converges well both for weak and strong couplings. Beyond a critical value of λ there is also a time-dependent, extremal instanton path associated with the tunneling of atoms between equivalent minima in the effective atomic potential. Assuming that the instantons are dilute a perturbation expansion of the electronic self-energy in terms of unrenormalized instanton propagators has been carried out and shown that for most purposes only the lowest-order, bare term has to be included.

We found that the usual Migdal-Eliashberg perturbation expansion breaks down around $\lambda \sim 1.25$. This breakdown is caused by the appearance of more than one extremal path of the action. Related to this is that the original expansion point at $\tilde{\phi} = 0$ for the phonon field $\tilde{\phi}$

corresponds no longer to a minimum but to a local maximum of the effective potential. The following picture emerges from the calculations: For $\lambda < 1.2$ the system is in a metallic state which can be described by Migdal-Eliashberg theory. Phonon renormalizations are then weak and the electronic mass enhancement is linear in λ . For $\lambda > 1.2$ the adiabatic approximation breaks down. The system stays mainly in ionic states with either two or zero electrons. Each state has its own displacement pattern and instantaneous equilibrium position. The system is still metallic due to atomic tunneling processes between the potential minima, however, the electronic spectral functions develop a two-peak structure which cannot be obtained in the Migdal-Eliashberg theory. Increasing λ further the electronic band splits into two subbands, the system becomes effectively insulating and behaves like a mixture of unoccupied and doubly occupied states. The semiclassical treatment and also the exact solution for vanishing hopping show that this “insulating” state is for any finite temperature not truly insulating: The density of electronic states between the two subbands is exponentially small but not exactly zero.

Acknowledgement: Both authors thank S. Ciuchi for stimulating and useful discussions. The first author acknowledges useful discussions with E. Cappelluti.

REFERENCES

¹ T. Holstein, Ann. Phys. **8**, 325 (1959); **8**, 343 (1959)

² D. Emin, Adv. Phys. **22**, 57 (1973)

³ V.V. Kabanov, O.Yu. Mashtakov, Phys. Rev. B **47**, 6060 (1993)

⁴ H. Fehske, J. Loos and G. Wellein, Z. Phys. B **104**, 619 (1997)

⁵ S. Ciuchi, F. de Pasquale and D. Feinberg, Europhys. Lett. **30**, 151 (1995)

⁶ S. Ciuchi, F. de Pasquale, S. Fratini and D. Feinberg, Phys. Rev. B **56**, 4494 (1997)

⁷ *Polarons and Bipolarons in High- T_c Superconductors and Related Materials*,
ed. by F.K.H. Salje, A.S. Alexandrov and W.Y. Lians, Cambridge University Press, Cambridge (1995)

⁸ J.D. Lee and B.I. Min, Phys. Rev. B **55**, 12 454 (1997)

⁹ A.B. Migdal, Ž. Ėksp. Teor. Fiz., **34** (1958) 1438 (Sov. Phys. JETP, **7**, 999 (1958));
G.M. Eliashberg, Ž. Ėksp. Teor. Fiz., **38** (1960) 966 (Sov. Phys. JETP, **11**, 696 (1960))

¹⁰ M.E. Reeves, D.A. Ditmars, S.A. Wolf, T.A. Vanderah and V.Z. Kresin, Phys. Rev. B **47**, 6065 (1993)

¹¹ A.S. Alexandrov and N.F. Mott, *High Temperature Superconductors and other Superfluids*
Taylor & Francis, London (1994)

¹² I.G. Lang and Yu.A. Firsov, Sov. Phys. JETP, **16** 1301 (1963)

¹³ H. Fehske, H.Röder, G. Wellein and A. Mistriotis, Phys. Rev. B **51**, 16 582 (1995)

¹⁴ A. Georges, G. Kotliar, W. Krauth and M.J. Rozenberg Rev. Mod. Phys. **68**, 13 (1996)

¹⁵ W. Metzner and D. Vollhardt, Phys. Rev. Lett. **62**, 324 (1989)

¹⁶ J.K. Freericks, M. Jarrell and D.J. Scalapino, Phys. Rev. B **48**, 6302 (1993)

¹⁷ J.K. Freericks, Phys. Rev. B **48**, 3881 (1993)

¹⁸ J.K. Freericks, Phys. Rev. B **50**, 403 (1994)

¹⁹ J.K. Freericks, M. Jarrell, Phys. Rev. B **50**, 6939 (1994)

²⁰ J.K. Freericks, M. Jarrell and D.J. Scalapino, Europhys. Lett. **25**, 37 (1994)

²¹ A.J. Millis, R. Müller and Boris I. Shraiman Phys. Rev. B **54**, 5389 (1996)

²² A.J. Millis, R. Müller and Boris I. Shraiman Phys. Rev. B **54**, 5405 (1996)

²³ E.N. Economou *Green's Functions in Quantum Physics*

Springer-Verlag Berlin Heidelberg New York (1979)

²⁴ A. Muramatsu and R. Zeyher, Nuclear Physics B **346**, 387 (1990)

²⁵ D.R. Hamann, Phys. Rev. B **2**, 1373 (1970)

²⁶ A.M. Polyakov, Nuclear Physics B **120**, 429 (1977)

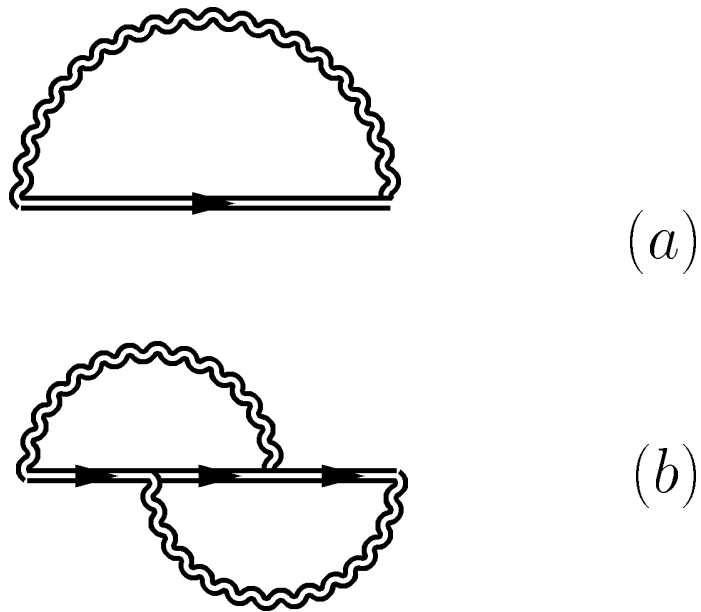


FIG. 1. Skeleton graphs for the electronic self-energy of second (a) and fourth order (b) in g .

The double solid lines denote the dressed electronic Green's function and the double wavy lines denote the full phonon propagator.

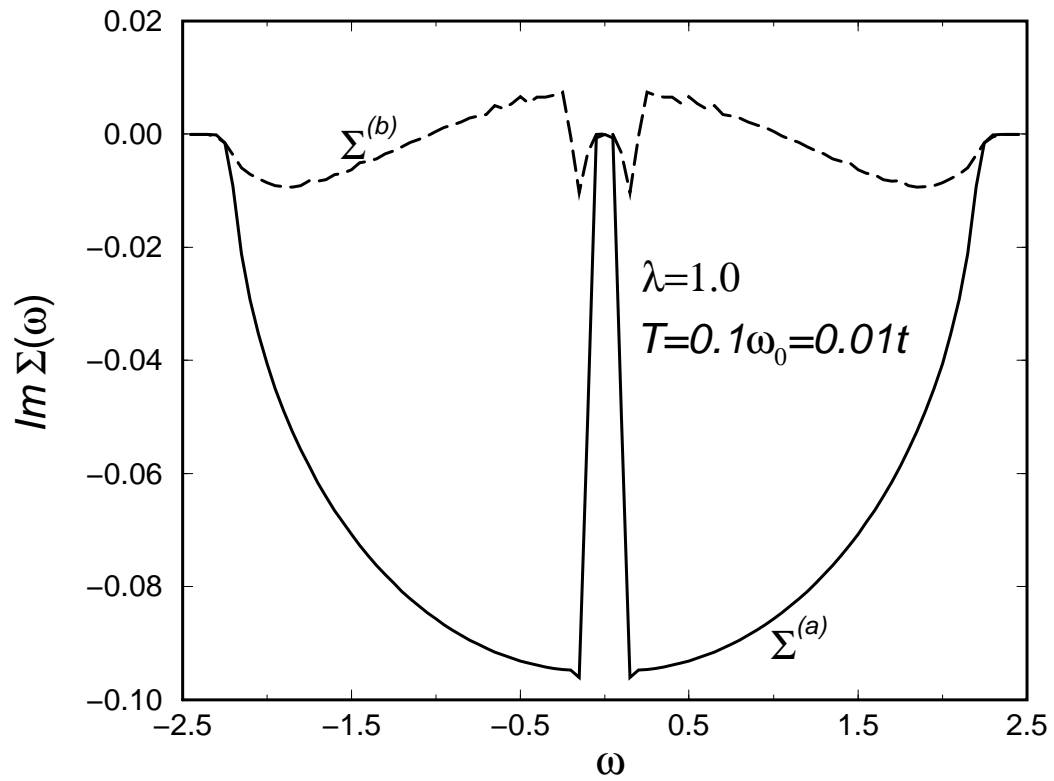


FIG. 2. Imaginary part of electronic self-energy contributions versus frequency for $\lambda = 1.0$. The solid line refers to the diagram (a) and the dashed line to the diagram (b) of Fig.1.

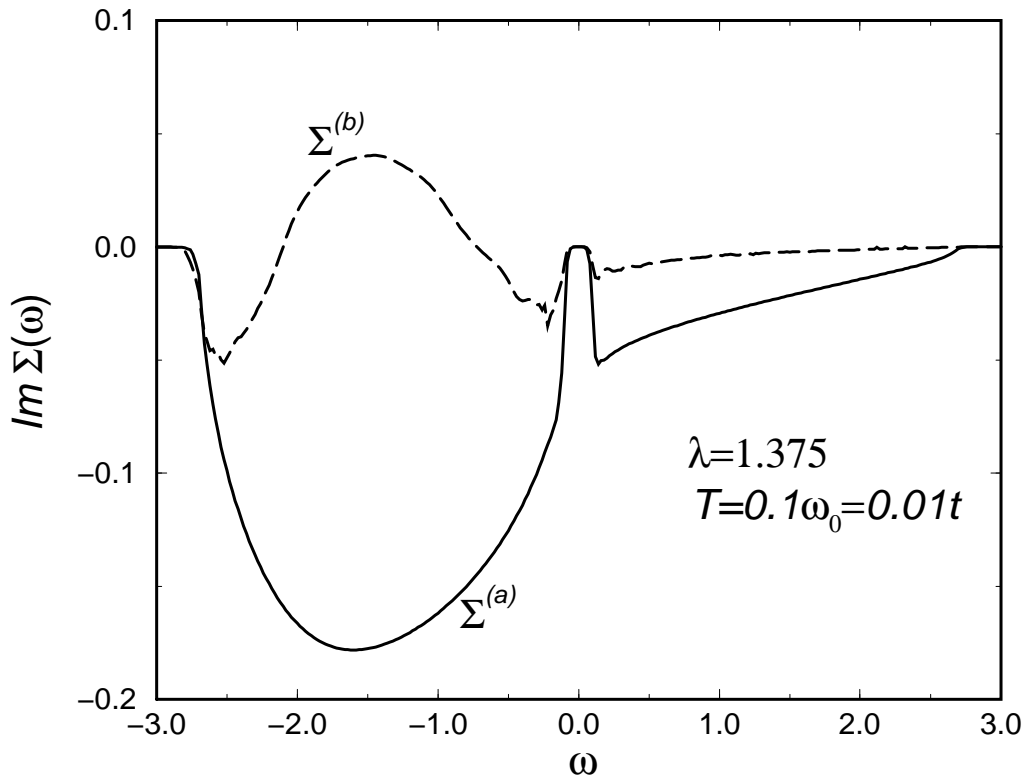


FIG. 3. Imaginary part of electronic self-energy contributions versus frequency for $\lambda = 1.375$.

The solid line refers to the diagram (a) and the dashed line to the diagram (b) of Fig.1.

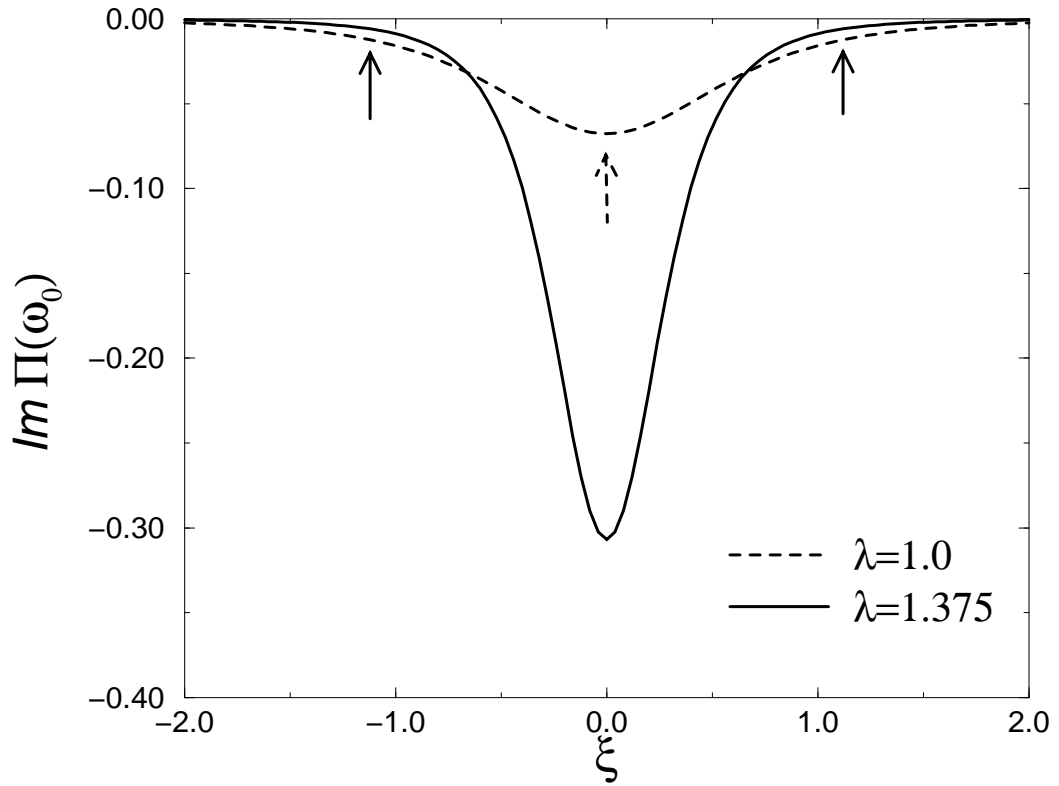


FIG. 4. Imaginary part of the phonon self-energy $\Pi(\omega_0)$ as a function of the dimensionless field $\xi = \tilde{\phi} \omega_0 / t^{1/2}$ for $T = 0.1\omega_0 = 0.01t$. The arrows show the correspondent position of the minima of the local effective potential.

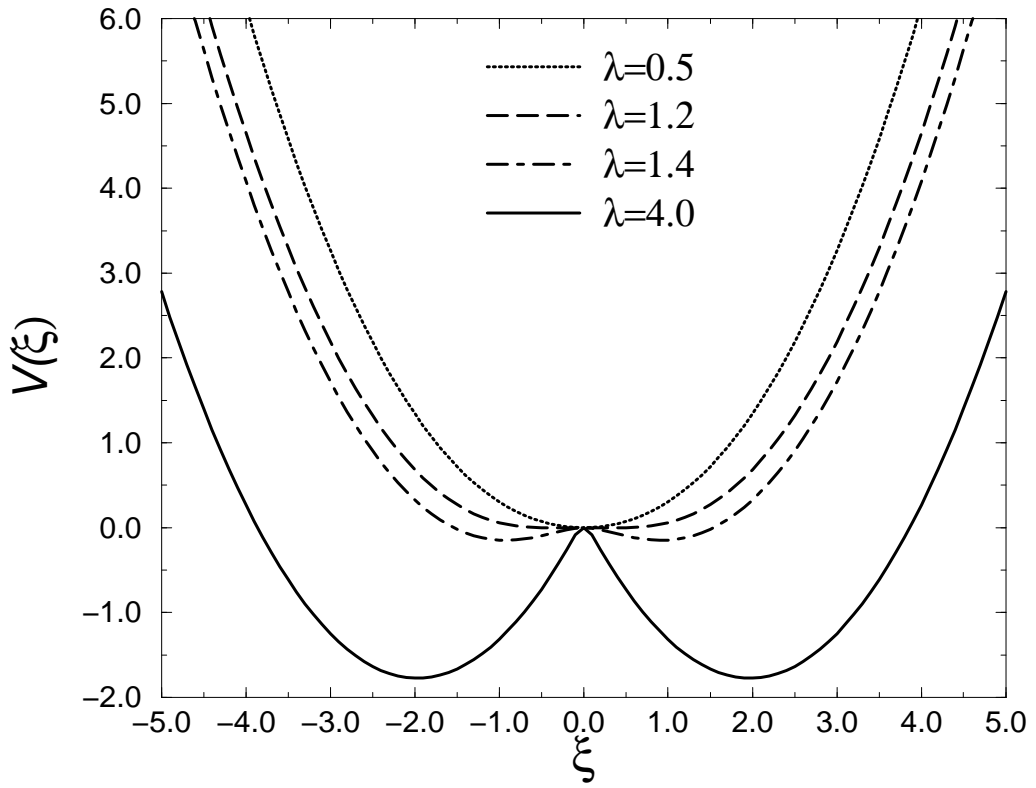


FIG. 5. Effective potential V of the atom versus the dimensionless phonon field $\xi = \tilde{\phi} \omega_0 / t^{1/2}$ for $T = 0.1\omega_0 = 0.01t$ and different λ 's.

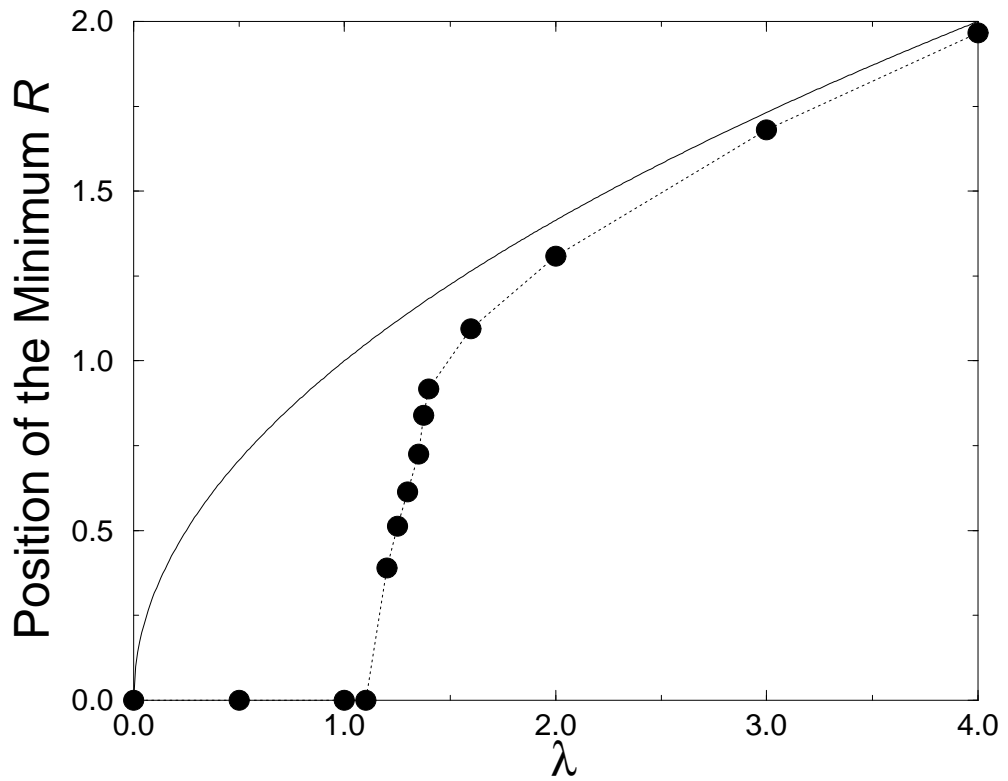


FIG. 6. Dotted line with circles: Position of the potential minimum R as a function of λ , for $T = 0.1\omega_0 = 0.01t$. Solid line: Asymptotic $\lambda^{1/2}$ dependence for vanishing hopping.

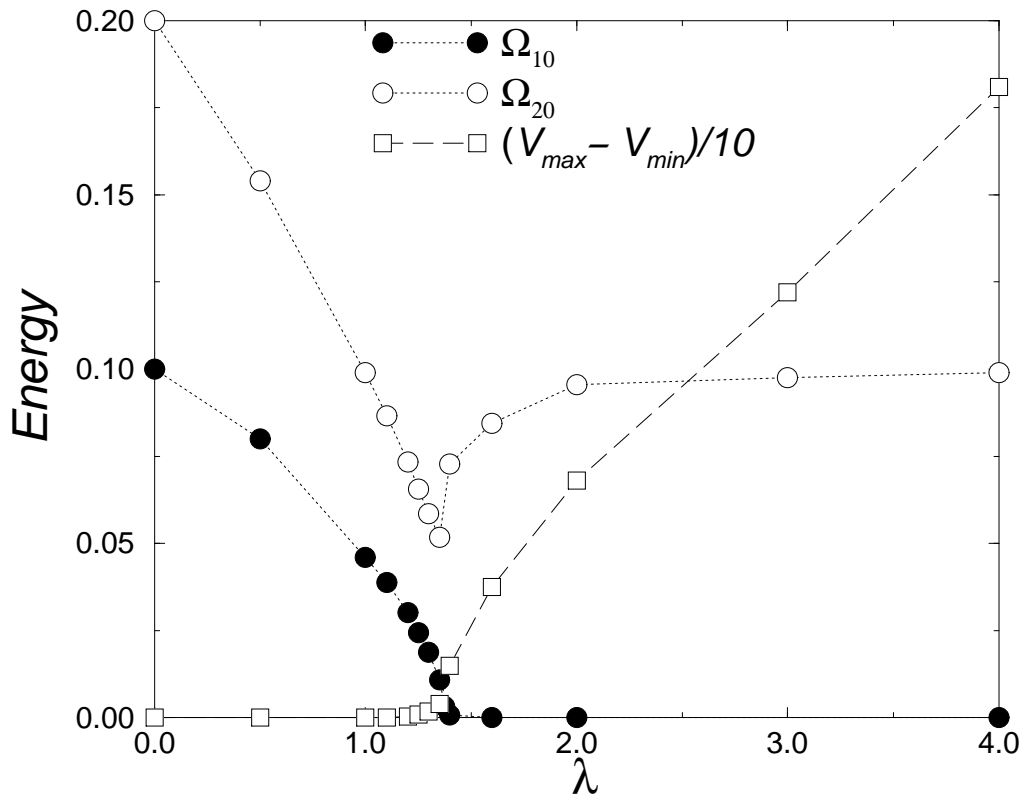


FIG. 7. Potential barrier $V_{max} - V_{min}$ (squares) and energy differences between the ground state and the first (filled circles) and the second (empty circles) excited states of the effective potential as a function of λ for $T = 0.1\omega_0 = 0.01t$.

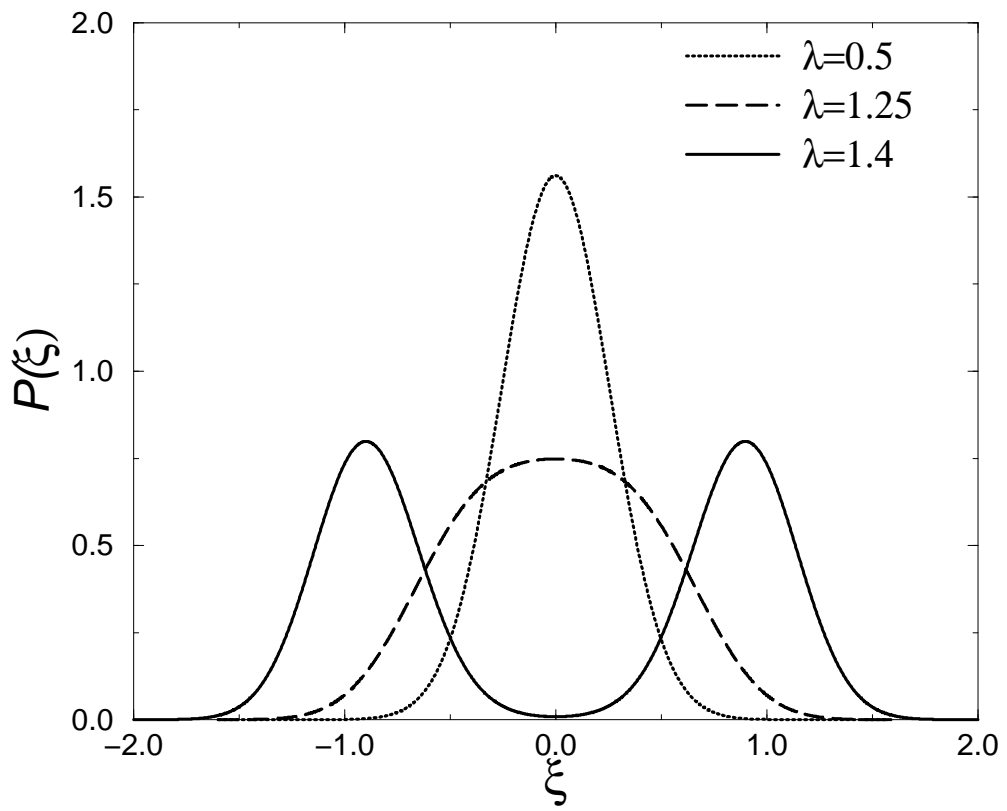


FIG. 8. Probability distribution P of the atom as a function of $\xi = \tilde{\phi} \omega_0 / t^{1/2}$ for $T = 0.1\omega_0 = 0.01t$ and three different values of λ .

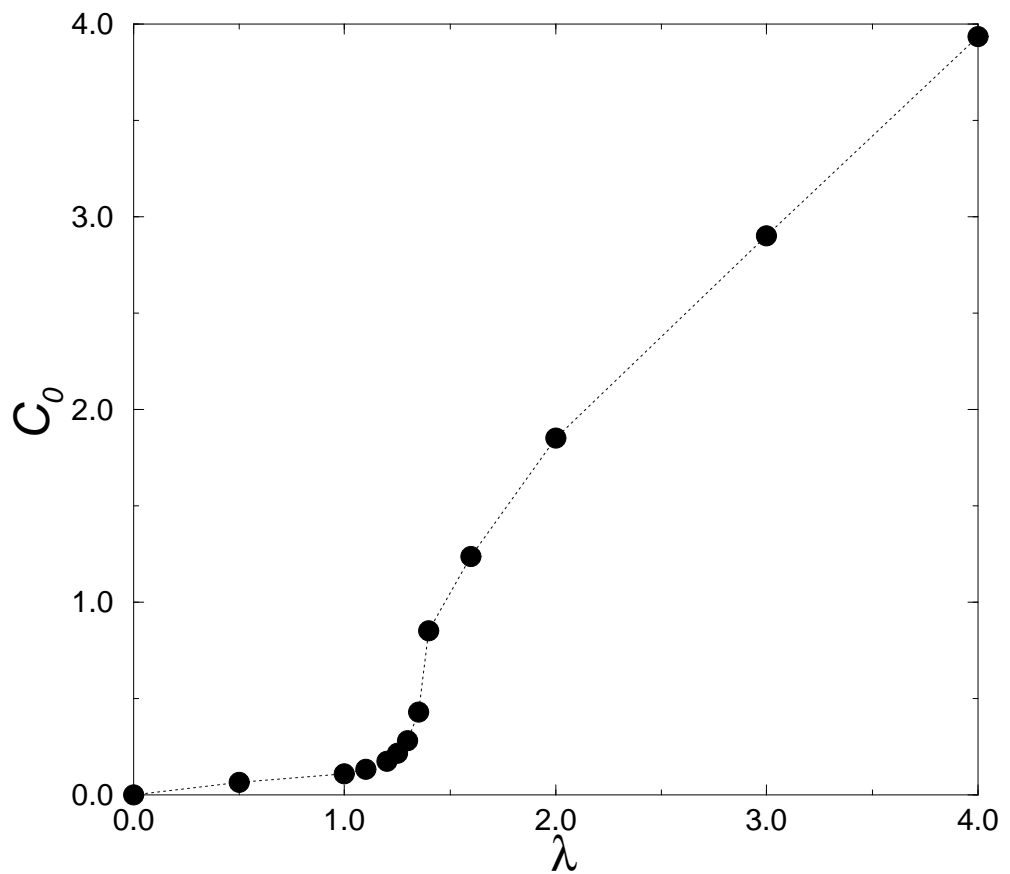


FIG. 9. Static electron-phonon correlation function $C_0 = -g/t \langle \tilde{\phi} n \rangle$ versus λ for $T = 0.1\omega_0 = 0.01t$.

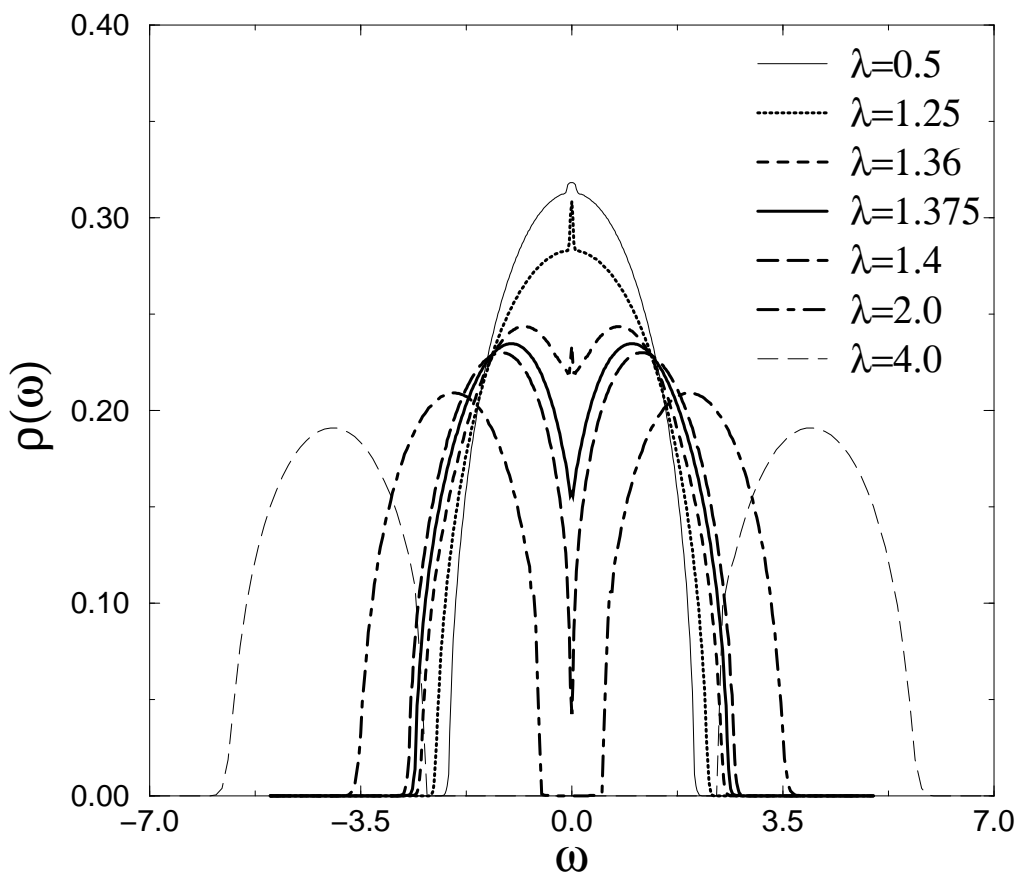


FIG. 10. Electronic density of states ρ versus frequency for $T = 0.1\omega_0 = 0.01t$ and different λ 's.

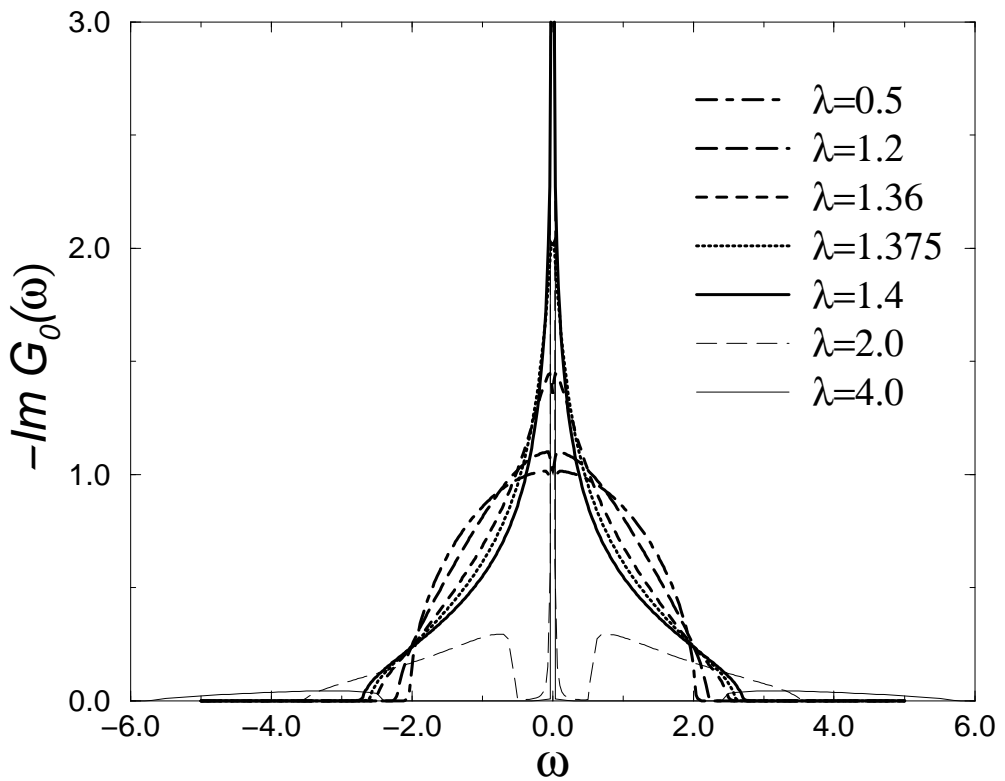


FIG. 11. Imaginary part of the "bare" electronic Green's function G_0 versus frequency for $T = 0.1\omega_0 = 0.01t$ and different λ 's.

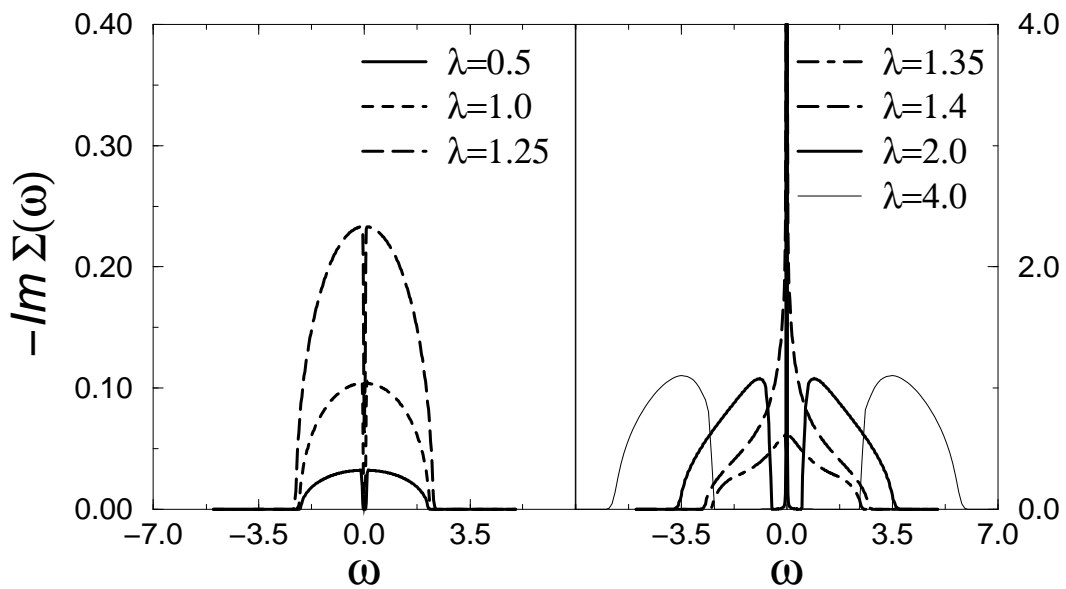


FIG. 12. Imaginary part of the electronic self-energy Σ versus frequency for $T = 0.1\omega_0 = 0.01t$.

The chosen values of λ extend from the weak- (a) to the strong-coupling (b) regime.

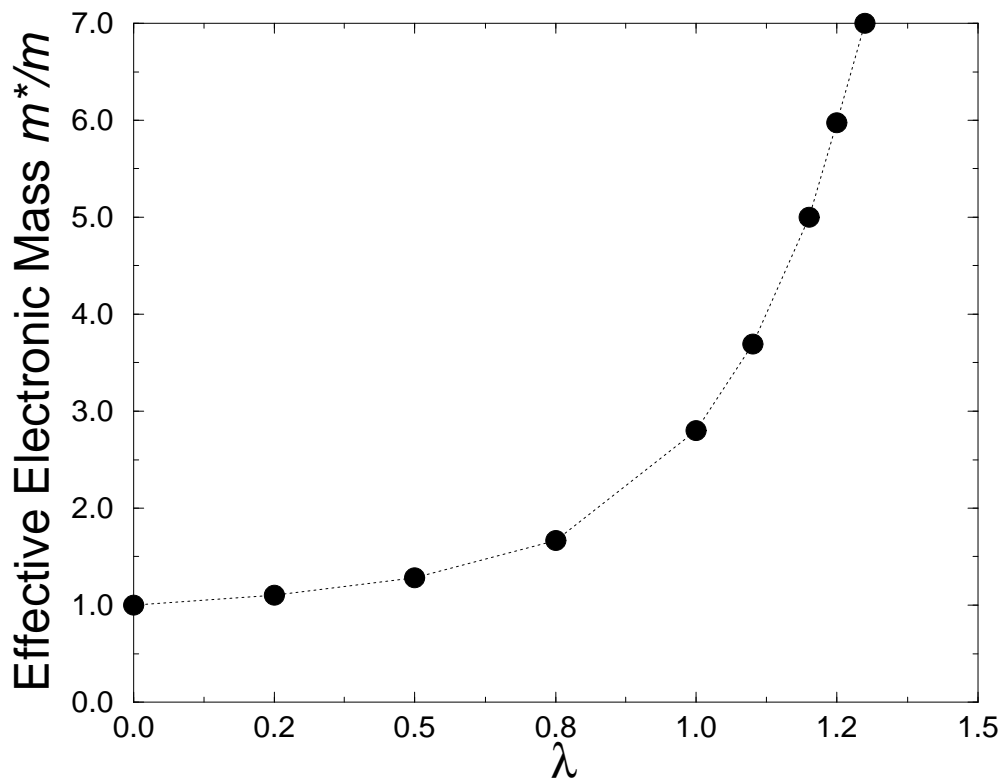


FIG. 13. Ratio of the effective and bare electronic mass versus λ for $T = 0.1\omega_0 = 0.01t$.

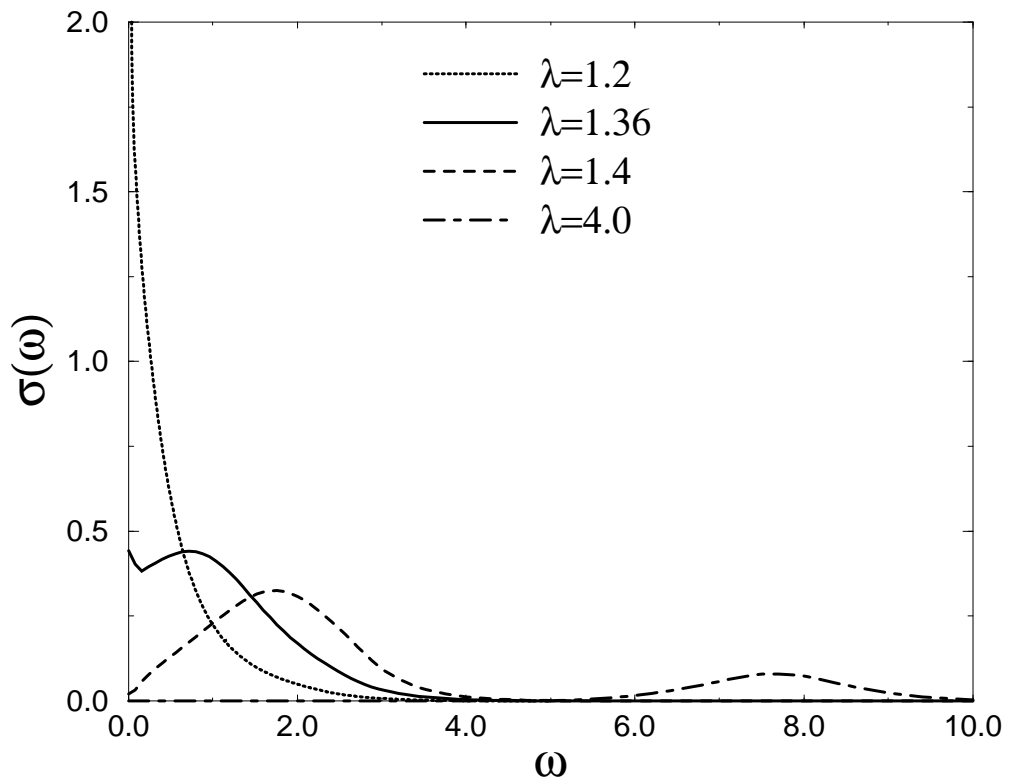


FIG. 14. Optical conductivity σ in arbitrary units as a function of the frequency for $T = 0.1\omega_0 = 0.01t$ and different λ 's.

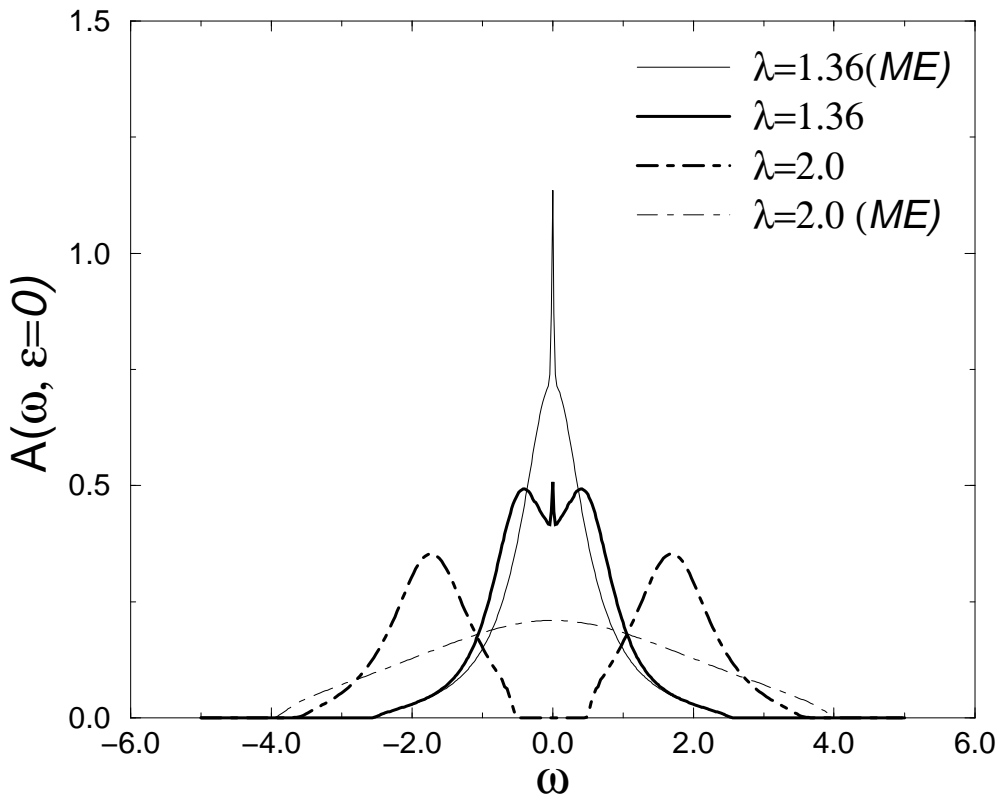


FIG. 15. One-particle spectral function A at the Fermi surface as a function of the frequency for $T = 0.1\omega_0 = 0.01t$. The thin solid and dot-dashed lines are calculated using the Migdal-Eliashberg theory, the corresponding thick lines are the present results.

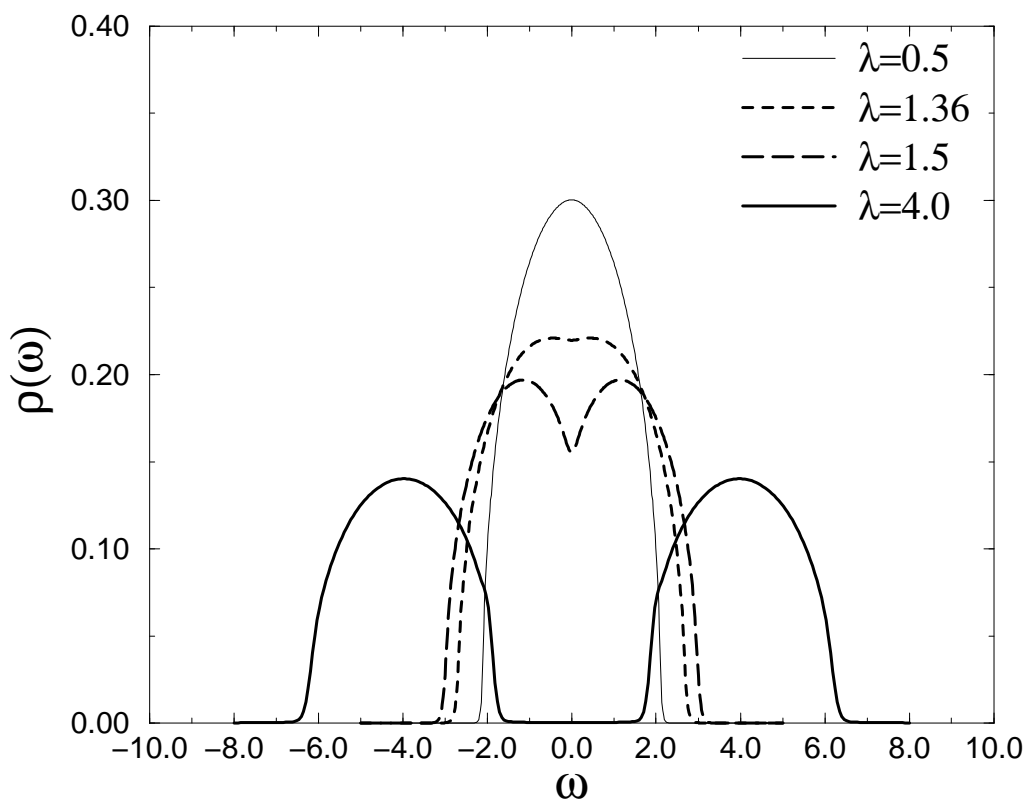


FIG. 16. Electronic density of states ρ versus frequency for $T = 2.0\omega_0 = 0.2t$ and different λ 's .

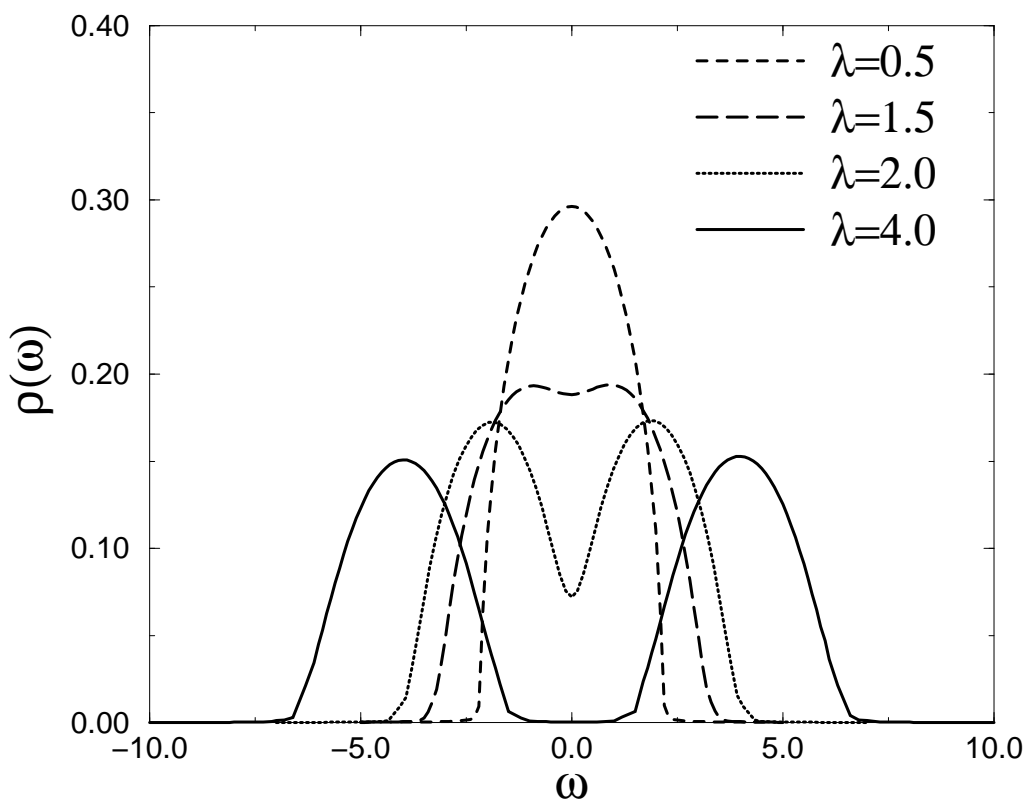


FIG. 17. Electronic density of state ρ versus frequency for $T = 2.0\omega_0 = 0.2t$ and different λ 's in the limit of classical, infinite heavy atoms.